Monthly Notices of the ROYAL ASTRONOMICAL SOCIETY

Mon. Not. R. Astron. Soc. **426,** 1574–1590 (2012) doi:10.1111/j.1365-2966.2012.21770.x

Gemini GMOS and WHT SAURON integral-field spectrograph observations of the AGN-driven outflow in NGC 1266

Timothy A. Davis,[1★] Davor Krajnović,[1] Richard M. McDermid,[2] Martin Bureau,[3] Marc Sarzi,[4] Kristina Nyland,[5] Katherine Alatalo,[6] Estelle Bayet,[2] Leo Blitz,[6] Maxime Bois,[7] Frédéric Bournaud,[8] Michele Cappellari,[2] Alison Crocker,[9] Roger L. Davies,[2] P. T. de Zeeuw,[1,10] Pierre-Alain Duc,[8] Eric Emsellem,[1,11] Sadegh Khochfar,[12] Harald Kuntschner,[13] Pierre-Yves Lablanche,[1,11] Raffaella Morganti,[14,15] Thorsten Naab,[16] Tom Oosterloo,[14,15] Nicholas Scott,[17] Paolo Serra,[14] Anne-Marie Weijmans[18]† and Lisa M. Young[5]‡

[1]*European Southern Observatory, Karl-Schwarzschild-Str. 2, 85748 Garching, Germany*
[2]*Gemini Observatory, Northern Operations Centre, 670 N. A'ohoku Place, Hilo, HI 96720, USA*
[3]*Sub-Department of Astrophysics, Department of Physics, University of Oxford, Denys Wilkinson Building, Keble Road, Oxford OX1 3RH*
[4]*Centre for Astrophysics Research, University of Hertfordshire, Hatfield, Herts AL1 9AB*
[5]*Physics Department, New Mexico Institute of Mining and Technology, Socorro, NM 87801, USA*
[6]*Department of Astronomy, University of California, Campbell Hall, Berkeley, CA 94720, USA*
[7]*Observatoire de Paris, LERMA and CNRS, 61 Av. de l'Observatoire, F-75014 Paris, France*
[8]*Laboratoire AIM Paris-Saclay, CEA/IRFU/SAp – CNRS – Université Paris Diderot, 91191 Gif-sur-Yvette Cedex, France*
[9]*University of Massachussets Amherst, Amherst, MA 01003 USA*
[10]*Sterrewacht Leiden, Leiden University, Postbus 9513, 2300 RA Leiden, the Netherlands*
[11]*Centre de Recherche Astrophysique de Lyon, Université Lyon 1, Observatoire de Lyon, Ecole Normale Supérieure de Lyon, 9 avenue Charles André, F-69230 Saint-Genis Laval, France*
[12]*Max-Planck Institut für extraterrestrische Physik, PO Box 1312, D-85478 Garching, Germany*
[13]*Space Telescope European Coordinating Facility, European Southern Observatory, Karl-Schwarzschild-Str. 2, 85748 Garching, Germany*
[14]*Netherlands Institute for Radio Astronomy (ASTRON), Postbus 2, 7990 AA Dwingeloo, the Netherlands*
[15]*Kapteyn Astronomical Institute, University of Groningen, Postbus 800, 9700 AV Groningen, the Netherlands*
[16]*Max-Planck-Institut für Astrophysik, Karl-Schwarzschild-Str. 1, 85741 Garching, Germany*
[17]*Centre for Astrophysics & Supercomputing, Swinburne University of Technology, PO Box 218, Hawthorn VIC 3122, Australia*
[18]*Dunlap Institute for Astronomy & Astrophysics, University of Toronto, 50 St. George Street, Toronto, ON M5S 3H4, Canada*

Accepted 2012 July 23. Received 2012 July 5; in original form 2012 June 13

ABSTRACT

We use the Spectrographic Areal Unit for Research on Optical Nebulae and Gemini Multi-Object Spectrograph integral-field spectrographs to observe the active galactic nucleus (AGN) powered outflow in NGC 1266. This unusual galaxy is relatively nearby ($D = 30$ Mpc), allowing us to investigate the process of AGN feedback in action. We present maps of the kinematics and line strengths of the ionized gas emission lines Hα, Hβ, [O III], [O I], [N II] and [S II], and report on the detection of sodium D absorption. We use these tracers to explore the structure of the source, derive the ionized and atomic gas kinematics, and investigate the gas excitation and physical conditions. NGC 1266 contains two ionized gas components along most lines of sight, tracing the ongoing outflow and a component closer to the galaxy systemic, the origin of which is unclear. This gas appears to be disturbed by a nascent AGN jet. We confirm that the outflow in NGC 1266 is truly multiphase, containing radio plasma, atomic, molecular and ionized gas and X-ray emitting plasma. The outflow has velocities of up to ± 900 km s^{-1} away from the systemic velocity and is very likely to remove

★E-mail: tdavis@eso.org
†Dunlap Fellow.
‡Adjunct Astronomer with NRAO.

© 2012 The Authors
Monthly Notices of the Royal Astronomical Society © 2012 RAS

Downloaded from http://mnras.oxfordjournals.org/ at European Southern Observatory on March 8, 2013

significant amount of cold gas from the galaxy. The low-ionization nuclear emission region-like line emission in NGC 1266 is extended, and it likely arises from fast shocks caused by the interaction of the radio jet with the interstellar medium. These shocks have velocities of up to 800 km s^{-1}, which match well with the observed velocity of the outflow. Sodium D equivalent width profiles are used to set constraints on the size and orientation of the outflow. The ionized gas morphology correlates with the nascent radio jets observed in 1.4 and 5 GHz continuum emission, supporting the suggestion that an AGN jet is providing the energy required to drive the outflow.

Key words: ISM: jets and outflows – galaxies: elliptical and lenticular, cD – galaxies: evolution – galaxies: individual: NGC 1266 – galaxies: ISM – galaxies: jets.

1 INTRODUCTION

In recent years the idea that feedback from an active galactic nucleus (AGN; e.g. Springel, Di Matteo & Hernquist 2005; Croton et al. 2006) could be responsible for quenching of star formation has grown in popularity. Such quenching seems to be required to create the red-sequence galaxies we observe today (e.g. Baldry et al. 2004). There is circumstantial evidence to support AGN-driven quenching, such as the study by Schawinski et al. (2007), suggesting that AGN are predominantly found in green valley galaxies, but direct evidence for removal/heating of cold star-forming gas is rare.

The physical mechanism by which an AGN could drive molecular gas out of a galaxy is still debated. Radiation pressure is thought to be important in star-formation-driven outflows (e.g. Murray, Quataert & Thompson 2005) and is potentially implicated in AGN-powered 'quasar mode' outflows (e.g. Arav et al. 1999; Kurosawa & Proga 2009). Kinetic feedback from an AGN jet can provide sufficient power to directly push through the interstellar medium (ISM) of a galaxy and entrain or destroy it (e.g. Rosario et al. 2010; McNamara & Nulsen 2012), but it is unclear if the geometry of a bipolar jet, which often emerges perpendicular to the nuclear disc, allows the jet to remove the ISM from an entire galactic disc. Broad-line winds can deposit significant momentum into gas surrounding an AGN, which could also lead to large outflows (e.g. Ostriker et al. 2010). Alternatively, heating by X-rays and cosmic rays could destroy/alter the molecular clouds close to an AGN, removing the need to expel them from the galaxy (e.g. Begelman, de Kool & Sikora 1991; Ferland et al. 2009). These processes should be distinguishable if we can identify and study local galaxies where AGN feedback is ongoing.

Our recent Combined Array for Research in Millimeter-wave Astronomy (CARMA) and Sub-Millimeter Array (SMA) observations of the nearby lenticular galaxy NGC 1266 suggest that it harbours a massive AGN-driven molecular outflow, providing an excellent local laboratory for studying AGN-driven quenching (Alatalo et al. 2011, hereafter A2011). NGC 1266 is a nearby ($D = 29.9$ Mpc; derived from recession velocity in Cappellari et al. 2011; hereafter ATLAS^{3D} Paper I), early-type galaxy (ETG) in the southern sky ($\delta = -2^{\circ}$), which was studied as part of the ATLAS^{3D} project. A three-colour image of this galaxy (from Kennicutt et al. 2003) is presented in Fig. 1. While typical CO spectra from ETGs reveal the double-horned profile characteristic of gas in a relaxed disc with a flat rotation curve, the spectrum of NGC 1266 shows a narrow central peak (full width at half-maximum ≈ 120 km s^{-1}) with non-Gaussian wings out to at least ± 400 km s^{-1} with respect to the systemic velocity (Young et al. 2011). Imaging of the high-velocity components using the SMA revealed that the wings resolve into red-shifted and blue-shifted lobes (A2011), coincident with Hα emission (Kennicutt et al. 2003), 1.4 GHz continuum (Baan & Klöckner 2006) and thermal bremsstrahlung emission (detected with *Chandra*; A2011; fig. 3). Molecular gas observations suggest that 3×10^8 $M_{\odot}$ of molecular gas is contained within the central 100 pc of NGC 1266 and that at least 5×10^7 $M_{\odot}$ of this gas is involved in a molecular outflow (A2011). This is thus the first observed large-scale expulsion of molecular gas from a non-starbursting ETG in the local Universe, and this presents a unique opportunity to study this powerful process in action.

In this paper we present the Spectrographic Areal Unit for Research on Optical Nebulae (SAURON) and Gemini Multi-Object Spectrograph (GMOS) integral-field unit (IFU) observations of the ionized gas in NGC 1266. By investigating the ionized gas kinematics and line ratios, we hope to constrain the outflow parameters and ionization mechanisms and thus shed light on the mechanism driving gas from the galaxy. In Section 2 we present the data and describe our reduction processes. We then present the derived maps of the gas kinematics and line fluxes. In Section 3 we discuss the kinematic structure of the system, gas excitation mechanisms and the driving force behind the outflow. Finally, we conclude and discuss prospects for the future in Section 4.

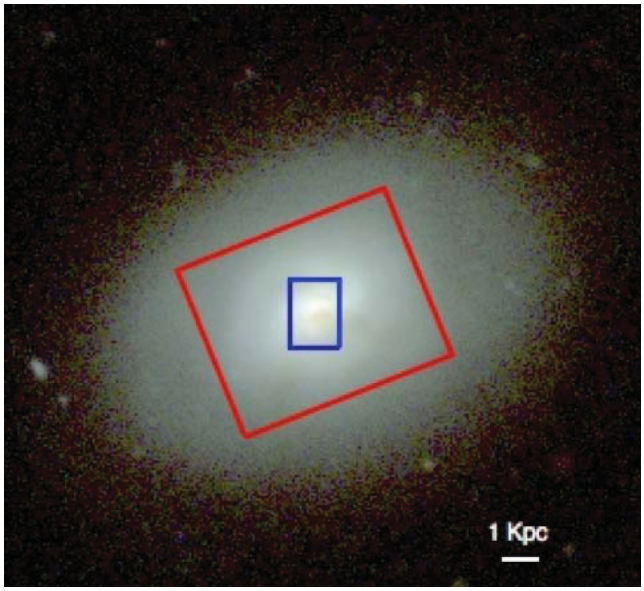

Figure 1. The Spitzer Infrared Nearby Galaxies Survey (SINGS; Kennicutt et al. 2003) *B*-, *V*- and *R*-band composite three-colour image of the S0 galaxy NGC 1266. The white bar shows a linear scale of 1 kpc (6.94 arcsec at an adopted distance of 29.9 Mpc; ATLAS^{3D} Paper I). Overlaid are the total FOV of our SAURON IFU (red) and GMOS IFU (blue) observations.

© 2012 The Authors, MNRAS **426,** 1574–1590
Monthly Notices of the Royal Astronomical Society © 2012 RAS

Downloaded from http://mnras.oxfordjournals.org/ at European Southern Observatory on March 8, 2013

2 DATA REDUCTION AND RESULTS

2.1 SAURON data

SAURON is an integral-field spectrograph built at the Lyon Observatory and mounted at the Cassegrain focus of the William Herschel Telescope (WHT). It is based on the TIGER concept (Bacon et al. 1995), using a microlens array to sample the field of view (FOV). Details of the instrument can be found in Bacon et al. (2001). The SAURON data of NGC 1266 were taken at the WHT, on the nights of 2008 January 10 and 11, as part of the ATLAS^{3D} observing campaign (ATLAS^{3D} Paper I). The galaxy was observed with the low-resolution mode of SAURON, covering an FOV of about 33 arcsec × 41 arcsec with 0.94 arcsec × 0.94 arcsec lenslets. The FOV of our observations is shown in red in Fig. 1. SAURON covers the wavelength range from 4810 to 5350 Å with a spectral resolution of 105 km s^{-1}.

The basic reduction of the SAURON observations was accomplished using the standard ATLAS^{3D} pipeline. Details of this process, including extraction of the stellar kinematics, are presented in Krajnović et al. (2011, hereafter ATLAS^{3D} Paper II). In brief, the two observed data cubes were merged and processed as described in Emsellem et al. (2004), using the Voronoi binning scheme developed by Cappellari & Copin (2003). This binning scheme maximizes the scientific potential of the data by ensuring a minimum signal-to-noise ratio of 40 per spatial and spectral pixel. This does however result in an non-uniform spatial resolution, here varying from 0.8 arcsec × 0.8 arcsec for unbinned spaxels in the central regions to 10 arcsec × 7 arcsec in the largest outer bin.

The SAURON stellar kinematics were derived using a penalized pixel fitting routine (Cappellari & Emsellem 2004), providing parametric estimates of the line-of-sight velocity distribution for each bin. During the extraction of the stellar kinematics, the GANDALF code (Sarzi et al. 2006) was used to simultaneously extract the ionized gas line fluxes and kinematics. The standard GANDALF reduction completed in the pipeline (using a single Gaussian for the lines) is insufficient in this source due to the complex structure of the ionized gas outflow (see Fig. 2). We have re-analysed the data cube using a multi-Gaussian technique (as described below) after the subtraction of the stellar continuum.

2.1.1 Emission line fitting

The SAURON spectra include the Hβ, [O III] and [N I] ionized gas spectral lines. As can be seen in Fig. 2, some of the binned spaxels show clear signs of having two ionized gas components along the line of sight with different velocities. In order to fit these profiles, we developed an IDL procedure based on the non-linear least-squares fitting code MPFIT (Markwardt 2009). In this procedure, we perform two fits and compare the chi-square to determine if two components are needed at each position.

In the first fit, we assume that a single ionized gas component is present, and fit the Hβ, [O III] and [N I] lines with single Gaussians. These Gaussians are constrained to have the same kinematics (velocity and velocity dispersion). Additionally, we confine the velocity of the lines to be within 1000 km s^{-1} of the galaxy systemic (2170 km s^{-1}; ATLAS^{3D} Paper I) and to have a velocity dispersion greater than the instrumental resolution, and less than a convolved velocity dispersion of ≈200 km s^{-1}. Initial guesses at the ionized gas kinematics were made by assuming that the ionized gas corotates with the stars, with a velocity dispersion of 120 km s^{-1}. We constrain the fitting by forcing each Gaussian to have a peak at least three times larger than the noise in the continuum, or to be zero.

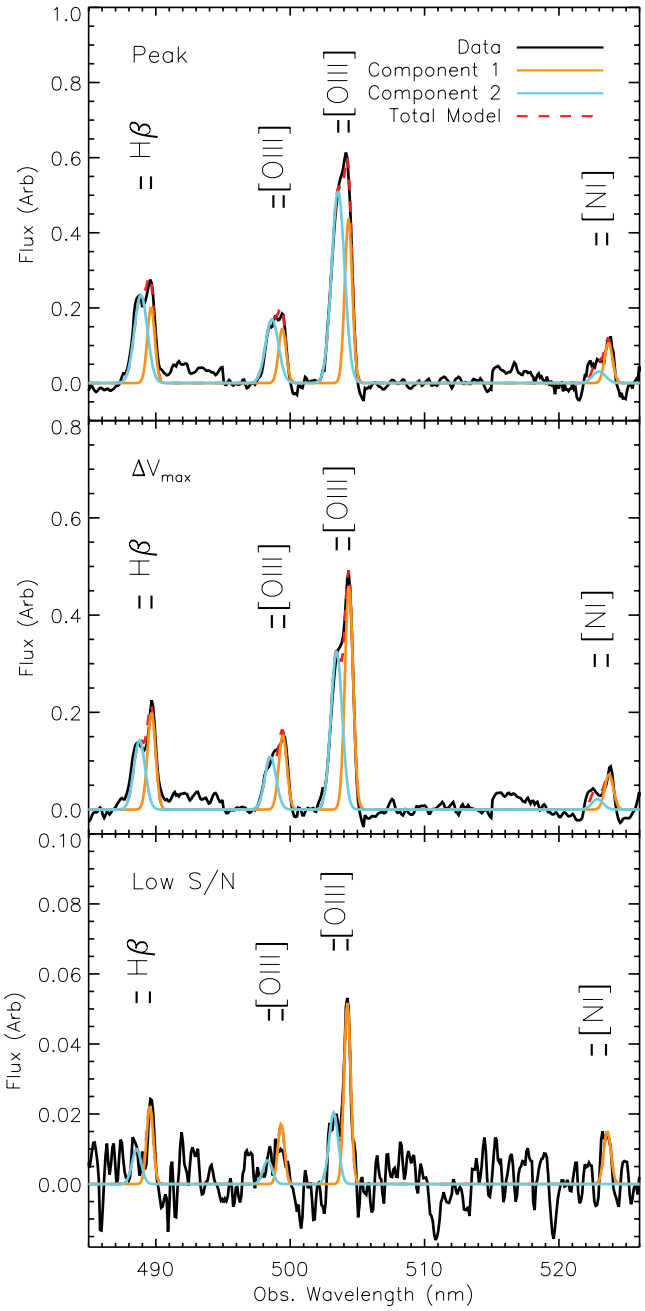

Figure 2. Stellar emission subtracted SAURON spectrum from single bins (black solid line) with line identifications. The top panel shows the spaxel with the largest line flux ($x = 0$ arcsec, $y = -4$ arcsec), the middle panel shows the spaxel with the biggest difference in the fitted velocities ($x = 0.8$ arcsec, $y = -5.17$ arcsec) and the bottom panel shows the lowest flux region where a two-component fit can be constrained ($x = -4.0$ arcsec, $y = -5.17$ arcsec). Overlaid is the two-component fit produced by an out-fitting routine, as described in Section 2.1.1. Component 1 (nearest the galaxy systemic) is shown in orange, while component 2 is shown in blue. The red dashed line shows the sum of components 1 and 2, which closely matches the observed data.

Any flux which had a 1σ error bar that included zero was set to zero. Initial guesses of the line fluxes were estimated by taking the maximum flux within the allowed velocity range of each line. The two [O III] lines in our spectral range have a fixed line ratio determined by the energy structure of the atom, and we fix the line ratio

Downloaded from http://mnras.oxfordjournals.org/ at European Southern Observatory on March 8, 2013

assumed in our fit to agree with the observed line ratio ($F_{5007} = 2.99 \times F_{4959}$; Storey & Zeippen 2000; Dimitrijević et al. 2007).

In the second fit, we assume that two independent ionized gas components are present in each bin and fit each component with its own set of independent linked Gaussians. As before, it is assumed that the lines in each component trace the same kinematics (velocity and velocity dispersion). Once again, we confine the velocity of each of the components to be within 1000 km s^{-1} of the galaxy systemic and to have a velocity dispersion greater than the instrumental resolution. We use different upper bounds for the first and second components of the gas distribution. Component 1 is forced to have a velocity dispersion less than 200 km s^{-1}, as before. In general, the second component is needed where the outflow is present and is thus allowed to have a higher velocity dispersion. We allowed the lines in the second component to have a maximum velocity dispersion of 360 km s^{-1}. In practice, however, good fits were found with velocity dispersions <300 km s^{-1}. The same limits were used on the line fluxes as described above.

Once the two fits described above were complete for each bin, we tested (using an F-test, as implemented in the MPFIT package; Markwardt 2009) if adding the additional free parameters to our model of the emission lines produced a significantly better fit; over and above the improvement expected when one adds free parameters. The F-test can be used as an indicator of where fitting two components produces better models, but the best threshold to take should be determined by visually inspecting the fits obtained (as the values tested for are at the extreme edge of the possible distribution). In this work, we visually chose a threshold that corresponds to an improvement in the chi-square of 60 per cent when adding in the additional parameters. When a spaxel did not satisfy this criterion, the values from the single Gaussian fit were used, and the second component was set to zero. Where two components were found to be necessary we denoted the component closest to the galaxy systemic as component 1 and the faster component as component 2.

In an attempt to ensure that the fits were robust, and spatially continuous, we implemented an iterative fitting regime where the fitting processes described above were performed for each spaxel in turn. Then the resulting two-dimensional flux and velocity maps were smoothed using a Gaussian kernel, and these smoothed values were used as the initial guesses for the next iteration of the fitting procedure. Using this procedure we found that the parameters usually converged within three iterations, with very little variance between fitting attempts. Fig. 2 shows SAURON spectra from a single bin, overlaid with the two-component fit. The top panel shows the spaxel with the largest line flux, the middle panel shows the spaxel with the biggest difference in the fitted velocities and the bottom panel shows the lowest flux region where a two-component fit can be constrained. Clearly, in the low-flux regions of the cube the fitted velocities are driven by the [O III]$_{5007}$ line, and the parameters have correspondingly higher uncertainties.

In Fig. 3, we show the observed kinematics for component 1 (panels a and b) and component 2 (panels c and d). The velocity dispersion maps have had the instrumental dispersion quadratically subtracted. We also show the stellar velocity field derived from these SAURON observations (panel e) for reference, as presented in ATLAS^{3D} Paper II. In Fig. 4 we show the fitted line fluxes.

2.2 Gemini GMOS data

In addition to the SAURON data, we obtained Gemini GMOS IFU observations of the central parts of NGC 1266, providing a higher spatial resolution and a longer wavelength coverage. The GMOS IFU uses a lenslet array of 1500 elements to feed individual positions on the sky to optical fibres (Allington-Smith et al. 2002; Hook et al. 2004). The total FOV of the IFU is 5 arcsec × 7 arcsec, with a spatial sampling of 0.2 arcsec. The Gemini GMOS IFU observations of NGC 1266 were taken over the nights of 2009 January 24, 26 and 27 at the Gemini North telescope (programme GN-2008B-DD-1). We used a four-point dither pattern to extend our coverage to a total FOV of ≈9.1 arcsec × 12.5 arcsec around the optical centre of the galaxy. The resultant FOV of our observations is shown in blue in Fig. 1. The low-resolution R150 grating was used, resulting in a spectral resolution of ≈185 km s^{-1} (at 6500 Å) over the wavelength range 5000–7300 Å. Two different blaze wavelengths (688 and 700 nm) were used on different exposures to allow continuous spectral coverage by averaging over chip gaps/bridges.

In order to reduce the GMOS IFU data we utilized a data reduction pipeline, as used in van de Ven et al. (2010). This pipeline calibrated and flat-fielded the data before they were trimmed and resampled into a homogeneous data cube. This cube was binned using the Voronoi binning technique of Cappellari & Copin (2003), ensuring a signal-to-noise ratio of 40 per spatial and spectral pixel. Due to the low spectral resolution and the depth of the exposures, we detected line emission to high significance over almost the entire IFU cube but were unable to detect stellar absorption features to high significance. As we are interested in the ionized gas kinematics in this work, we simply wish to remove the (relatively smooth) stellar continuum. We do this by fitting the stellar continuum with the penalized pixel fitting routine of Cappellari & Emsellem (2004), as used for our SAURON data. We were able to constrain the number of stellar templates required using our best fit to the SAURON data. Once the stellar continuum was successfully removed, we were left with a cube containing the ionized gas emission only.

The spectral range of our cube includes various ionized gas emission lines. The [O III] and [N I] are included in our GMOS spectrum in the region which overlaps with the SAURON spectral range. These lines however appear very weak because they are at the edge of our band pass, where the throughput is low. The main strong lines we detect are Hα, [N II]$_{6548,\,6583}$ and [O I]$_{6300}$, while He I and [N II]$_{5754}$ are detected more weakly. We choose to fit the kinematics of the gas emission on the strong lines only and impose these kinematics when measuring the fluxes of weaker lines. Example spectra extracted from the cube are shown in Fig. 5. We show here the region around the Hα, [N II] and [S II] lines only. These spectra were selected to lie at the spatial position with the highest line flux (top panel), the spaxel with the largest difference between the two fitted velocities (middle panel) and at the lowest flux bin in which we can constrain two components (bottom panel). With the low spectral resolution of this data, the lines are blended; however, we clearly require two components to fit the line emission. We also detect sodium D (NaD) absorption against the stellar continuum (an example spectrum is shown in Fig. 6). We describe the fitting procedure used for the gas emission lines in detail in Section 2.2.1 and the procedure used to measure the parameters of the NaD absorption in Section 2.2.2.

2.2.1 *Emission line fitting*

GMOS emission line fitting was carried out as described in Section 2.1.1, with some modifications described below. We fit here the Hα, [N II], [S II] and [O I] lines with single and double Gaussians. Initial guesses for the velocity and velocity dispersion were made

© 2012 The Authors, MNRAS **426,** 1574–1590
Monthly Notices of the Royal Astronomical Society © 2012 RAS

Downloaded from http://mnras.oxfordjournals.org/ at European Southern Observatory on March 8, 2013

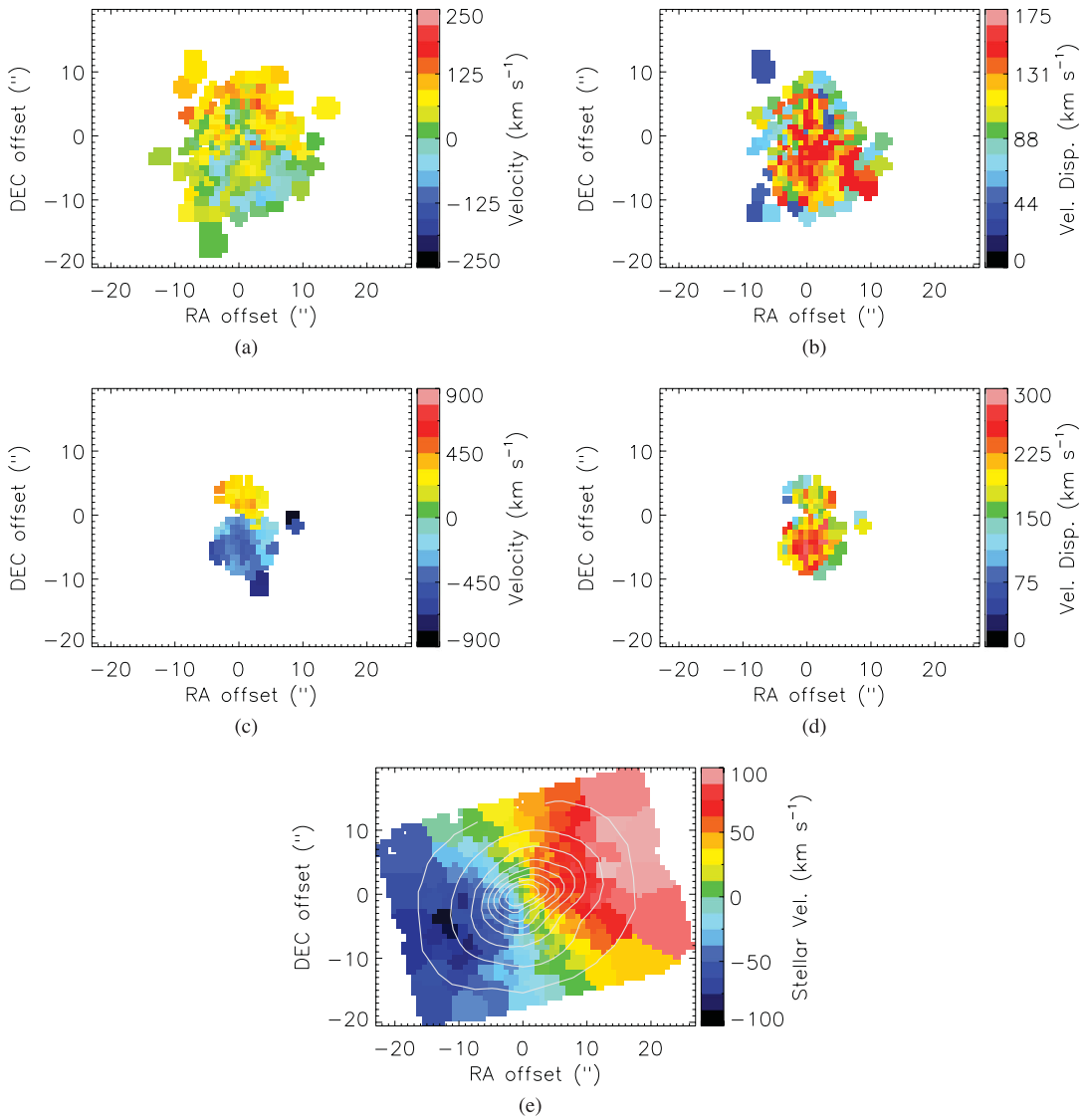

Figure 3. Ionized gas kinematics derived from the SAURON IFU data reduction process discussed in Section 2.1.1. In the top row (panels a and b) we display the kinematics of component 1 (confined to be closest to the galaxy systemic velocity). Bins where only one ionized gas component is required are also shown in component 1. The kinematics of the faster component is shown in the middle row (panels c and d). The ionized gas velocity is displayed in the left-hand panels (a, c) and the velocity dispersion in the right-hand panels (b, d). The stellar velocity field of this galaxy derived from these same observations in ATLAS^{3D} Paper II is shown as a comparison in panel e, with stellar continuum flux contours overlaid. These plots are centred around the galaxy position given in ATLAS^{3D} Paper I.

using the derived kinematics from the SAURON cube. The two [N II] lines in the Hα region of the spectrum have a fixed line ratio determined by the energy structure of the atom, and we forced the line ratios to the theoretical line ratio ($F_{6584} = 2.95 \times F_{6548}$; Acker 1989). The [S II] doublet is an electron density tracer, with the line ratio F_{6731}/F_{6717} varying from 0.459 at the high-density limit to 1.43 at the low-density limit (e.g. De Robertis, Dufour & Hunt 1987). Here we constrain the [S II] line ratio to lie somewhere within this region. We also allow the lines in the second component to have a maximum velocity dispersion of 500 km s^{-1}, but again note that good fits were found in most bins with velocity dispersions <300 km s^{-1}.

As for the SAURON data, to ensure that the fits were robust and spatially continuous, we implemented an iterative fitting regime where the fitting processes described above were performed multiple times, using a smoothed version of the output from the previous run as the initial condition. We found that the parameters usually converged within four iterations, again with very little variance between fitting attempts. Fig. 5 shows the GMOS spectra from a single bin (from the same spatial region as selected before), overlaid with the two-component fit, as found by this procedure.

In Fig. 7 we show the observed kinematics for component 1 (panels a and b) and component 2 (panels c and d). The velocity dispersion maps have had the instrumental dispersion quadratically subtracted. In Fig. 8 we show the fitted line equivalent widths (EWs) for the strong lines, with fitted component 1 in the top row and component 2 in the bottom row. We calculate the EW in the standard way by finding the width of a rectangle, with a height which is the same as the average stellar continuum flux in the region of the lines, which has the same area as the observed lines. As the GMOS data were taken in non-photometric conditions, we will use only ratios of the line fluxes from this point on.

Downloaded from http://mnras.oxfordjournals.org/ at European Southern Observatory on March 8, 2013

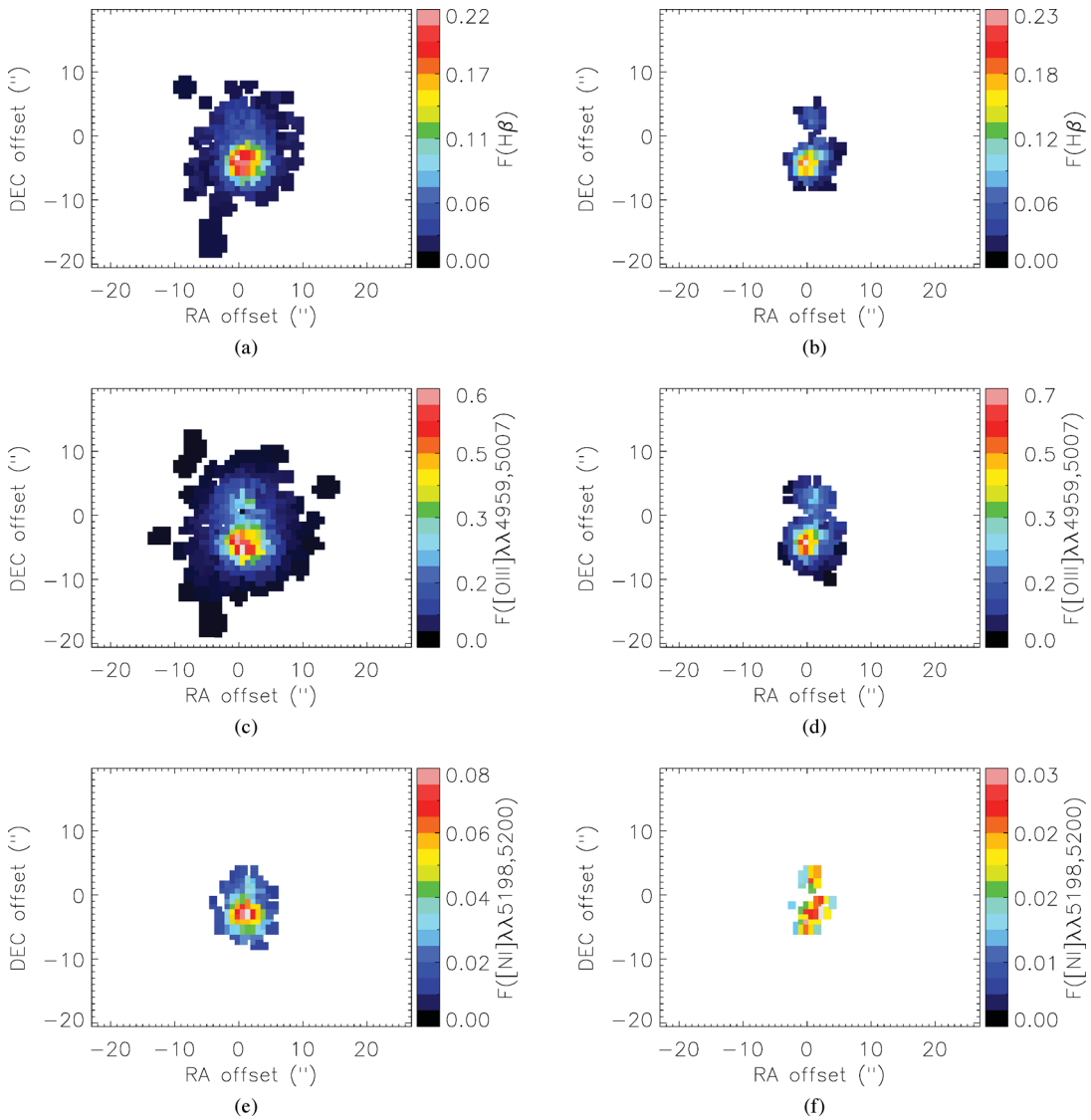

Figure 4. Ionized gas line fluxes derived from the SAURON IFU data reduction process discussed in Section 2.1.1. In the left-hand column we display the flux of component 1 (confined to be closest to the galaxy systemic). Bins where only one ionized gas component is required are also shown in component 1. The flux of the faster outflowing component is shown in the right-hand column. The top row shows the Hβ line fluxes (panels a and b), the second row the [O III] line fluxes (panels c and d) and the third row the [N I] fluxes (panels e and f). Fluxes are in units of 10^{-16} erg s^{-1} cm^{-2} arcsec^{-2} in each SAURON bin.

2.2.2 Absorption line fitting

The sodium absorption lines at 5890 and 5896 Å are detected in our GMOS IFU data (Fig. 6). This feature is unlikely to be due to an imperfect stellar template leaving negative residuals after subtraction from the GMOS spectrum, as the fitted velocities of the absorption feature do not match the stellar velocities assumed when fitting the template.

In order to extract the absorption depths and determine the neutral gas kinematics, we jointly fit the absorption doublet and the neighbouring He I emission line (and Na I skyline). We fix the velocity and velocity dispersion of the He I line using the best solution for each bin derived from the stronger lines (as described in Section 2.2.1). We then fit this line with two Gaussian components, as before, to determine the line fluxes.

Simultaneously, we fitted the NaD absorption doublet (which is blended in our data), assuming a Gaussian profile for both lines. Formally, an absorption line should be fitted with a Voigt profile, as the absorption has an intrinsic Lorentzian shape, which has been convolved with the instrumental Gaussian response. In the low-spectral-resolution data we present here, however, we fit Gaussian profiles, as the instrument response function is much broader than the intrinsic absorption. If one fits a Voigt profile to our data, the best-fitting profiles always tend towards a pure Gaussian, with a Lorentzian width (Γ) of zero, validating such an approach. We do not fix the NaD velocity and velocity dispersion, as the absorption arises from a different gas phase, which may have different kinematics (see Section 3.2). The velocities of the NaD hosting gas are constrained in our fit to lie within 1000 km s^{-1} of the systemic velocity, and the velocity dispersion of this component is constrained to be greater than the instrumental but less than 500 km s^{-1}. At the spectral resolution of our data, we only require a single neutral gas component in all spaxels in order to fit the absorption profiles well.

In Fig. 9 we show the observed absorption EW and the kinematics for the NaD absorbing gas. We calculate the EW in the standard way, as above.

© 2012 The Authors, MNRAS **426,** 1574–1590
Monthly Notices of the Royal Astronomical Society © 2012 RAS

Downloaded from http://mnras.oxfordjournals.org/ at European Southern Observatory on March 8, 2013

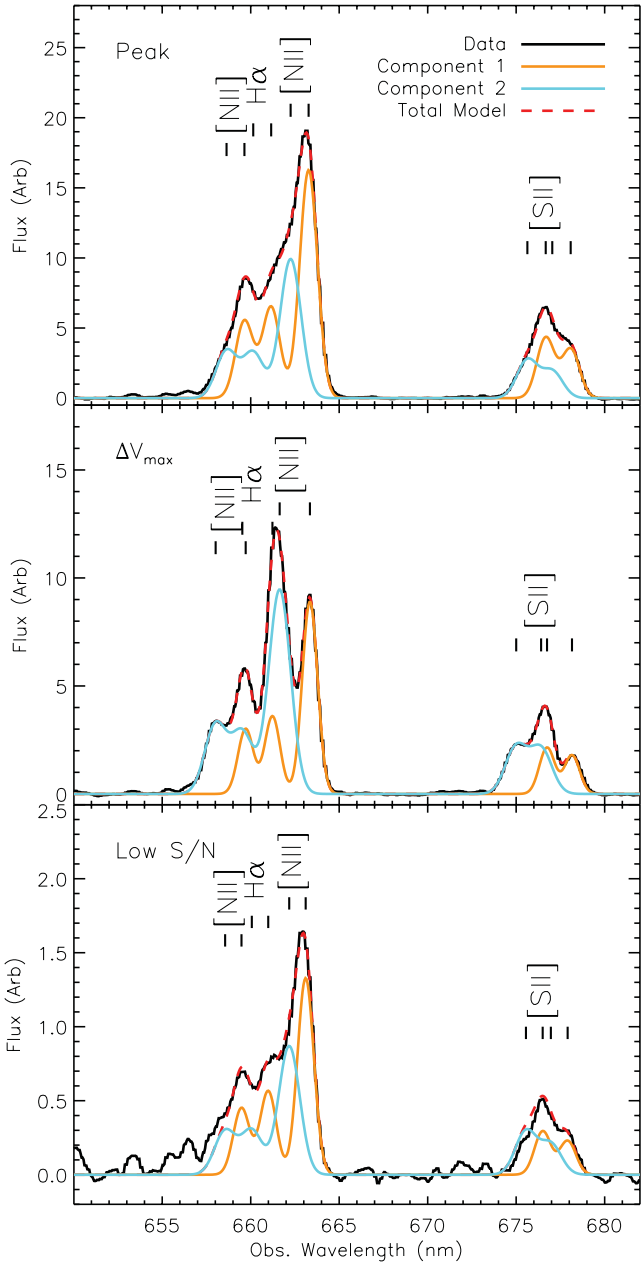

Figure 5. Stellar subtracted GMOS spectrum (black solid lines) from single bins with line identifications. The top panel shows the bin with the spaxel with the peak line flux ($x = 0.91$ arcsec, $y = -2.08$ arcsec), the middle panel shows the spaxel with the largest difference between the two fitted velocities ($x = -0.2$ arcsec, $y = -4.29$ arcsec) and the bottom panel shows the bin with the lowest total flux in which we are able to fit two components ($x = -1.85$ arcsec, $y = -5.73$ arcsec). Overlaid is the two-component fit produced by an out-fitting routine, as described in Section 2.2. Component 1 (nearest the galaxy systemic) is shown in orange, while component 2 is shown in blue. The red dashed line shows the sum of components 1 and 2, which closely matches the observed data.

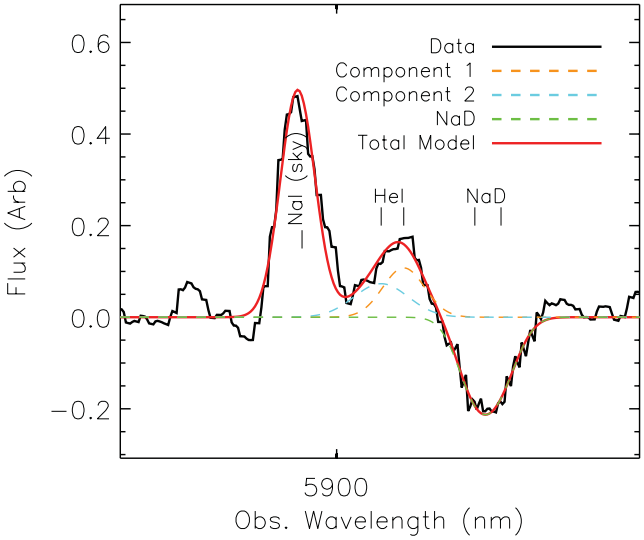

Figure 6. GMOS spectrum of the NaD region from a single bin ($x = -1.0$ arcsec, $y = -1.8$ arcsec; black solid line). Overlaid is the two-component fit produced by our fitting routine for the emission lines, as described in Section 2.2. Component 1 (nearest the galaxy systemic) is shown in orange, while component 2 is shown in blue. The red line shows the sum of components 1 and 2 (and our fit to the Na I skyline), which closely matches the observed data. Shown in green is our fit to the NaD absorption trough.

3 DISCUSSION

3.1 Ionized gas emission line kinematics

Figs 3 and 7 show the ionized gas kinematics derived from our multi-Gaussian fitting procedure. The SAURON data have a much wider FOV, providing insight into the large-scale kinematics of this object. The GMOS IFU data zoom in to the central portions of this object to reveal the inner regions.

Panel a of Fig. 3 shows the SAURON ionized gas kinematics for the component nearest the galaxy systemic velocity (which we will hereafter call the *systemic* component). This component includes gas out to a radius of ≈10 arcsec (1.5 kpc). A2011 discussed the molecular gas distribution and found evidence for a rotating molecular disc, as well as a molecular outflow. The origin of this systemic component and its relation to the molecular disc are unclear. This component could be due to unrelated gas components at different locations along the line of sight, or it may be a coherent structure which has been disturbed.

Some degree of symmetry appears to exist in the gas distribution around a line inclined ≈20° from east. This may suggest some bulk rotation, with a kinematic position angle of ≈30°. If this component is rotating, then comparison with the stellar rotation (shown in the bottom row of Fig. 3) shows that it is misaligned from the stellar rotation by ≈90°, suggesting that it could be in the polar plane. In the inner ≈6 arcsec, however, the velocity field changes sign and is disturbed.

Fig. 7 shows the GMOS zoomed in view of the centre of NGC 1266. The same disturbed features presented in the SAURON data are observed in the GMOS velocity field (panel a of Fig. 7). These features persist whatever our choice of initial velocities for the fitting procedure and are located at the same spatial location as the most blue- and red-shifted gas in component 2. When fitting multiple components to observed velocity profiles, it is always possible that such reversed sign velocity structures are a result of misfitting or overfitting of the line components. Here however we find the same structure from both the SAURON and GMOS data independently. Our iterative fitting procedure described in Sections 2.1.1 and 2.2.1 is designed to avoid discontinuous fits, and thus tries to remove such disturbed structures, but is unable to find better fits in these spaxels. The middle panels of Figs 2 and 5 show the emission

Downloaded from http://mnras.oxfordjournals.org/ at European Southern Observatory on March 8, 2013

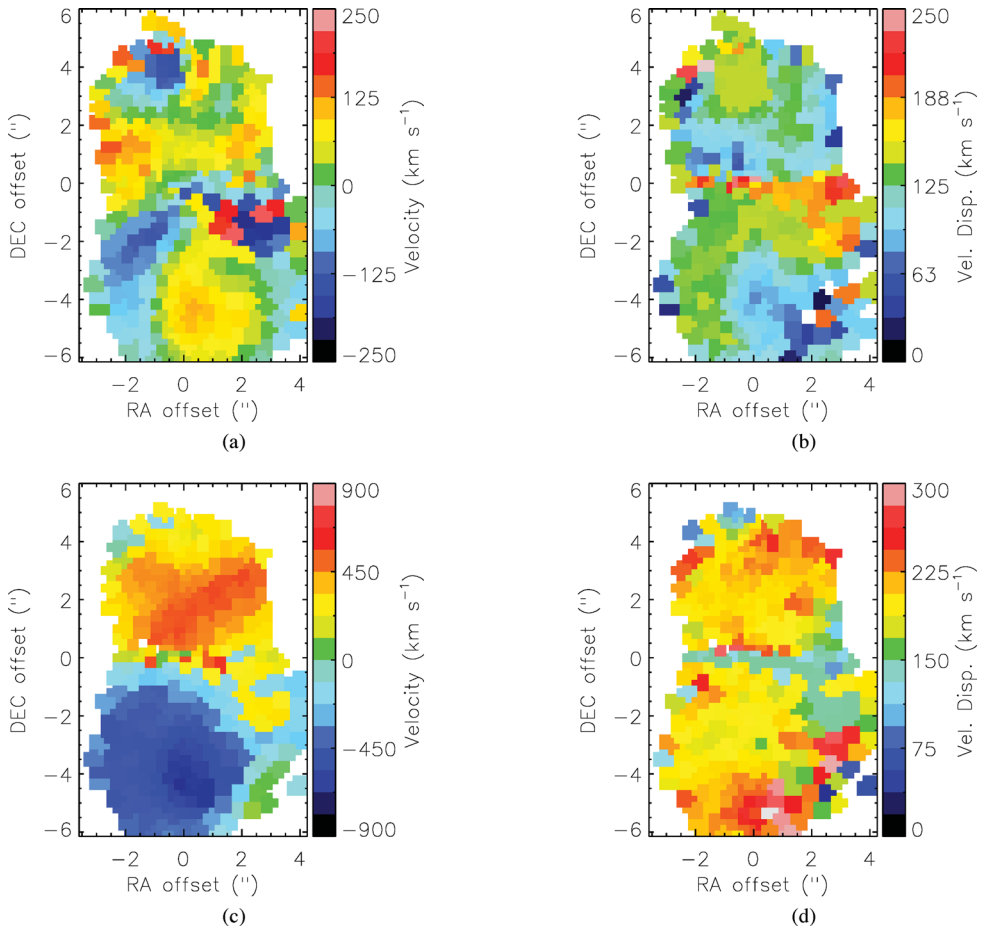

Figure 7. Ionized gas kinematics derived from the GMOS IFU data reduction process discussed in Section 2.2. In the top row (panels a and b) we display the kinematics of component 1 (confined to be closest to the galaxy systemic). Bins where only one ionized gas component is required are also shown in component 1. The kinematics of the faster outflowing component are shown in the bottom row (panels c and d). The ionized gas velocity is displayed in the left-hand panels and the velocity dispersion in the right-hand panels.

line spectrum in the bin with the largest blue-shifted velocity in each data set (where the disturbed systemic component is also detected). Clearly, the outer edges of each blended line or line complex (which drive our determination of the relative velocities of the two components) are well fitted, increasing our confidence that this structure is real.

If the systemic component is a misaligned rotating structure, then we speculate that the disturbance visible in the inner parts could be where the molecular outflow detected in A2011 has punched through, and material is flowing inwards to fill the vacuum. Given the dynamical time-scale of gas at this radius (≈30–40 Myr; A2011), it is difficult to imagine that the disturbed gas in the centre of this object could exist for long without being smeared out. This suggests that either this feature is very young or we are indeed observing unrelated clouds along the line of sight, which are not dynamically linked. A2011 estimate the age of the molecular outflow in this object as ≈2.6 Myr, so a recent cause of this feature is not completely ruled out. Alternatively, if these are unrelated clouds along the line of sight, the blue features to the south of the nucleus may be directly related to the outflow. Close correlation between some of these features and the radio jet supports this conclusion (see Section 3.5). Higher spatial resolution observations would allow us to disentangle these two possibilities.

Panel c of Fig. 3 shows the global SAURON view of the gas kinematics where a second component was required. This gas appears to be in a two-lobed structure, orientated approximately north–south (misaligned from the kinematic axis of the stars by ≈70°; ATLAS^{3D} Paper II). The gas in this component has velocities of up to ≈800 km s^{-1} away from the systemic velocity. We denote this component as the *outflow* from this point. Panel c of Fig. 7 shows this component in more detail. With finer spatial sampling of the GMOS IFU map, we are able to detect gas with velocities of up to ≈900 km s^{-1} away from the systemic velocity. As argued in A2011, the escape velocity in the centre of this object is at most ≈340 km s^{-1} supporting the idea that the outflow in this system allows material to escape the galaxy. The molecular gas in the outflow of this object reaches velocities of up to ≈480 km s^{-1}, with a slightly smaller spatial extent (see Fig. 10). This could suggest that molecular gas is destroyed as it flows out of the galaxy or that our observations were not sensitive to detect emission from the molecular gas at the highest velocities.

The molecular gas in NGC 1266 dominates the total mass of the ISM (with a mass of $\approx 2 \times 10^9$ M$_\odot$) and is contained within the innermost ≈100 pc of the galaxy (A2011). It is very hard to explain how this gas lost its angular momentum when it was already present within the galaxy. Deep optical imaging shows some minor signatures that could be due to recent disturbances, but no signatures of a stellar bar (Duc et al., in preparation). A minor merger could explain the compactness of the gas if the merger happened with the correct initial parameters to leave the gas with little or no angular

Downloaded from http://mnras.oxfordjournals.org/ at European Southern Observatory on March 8, 2013

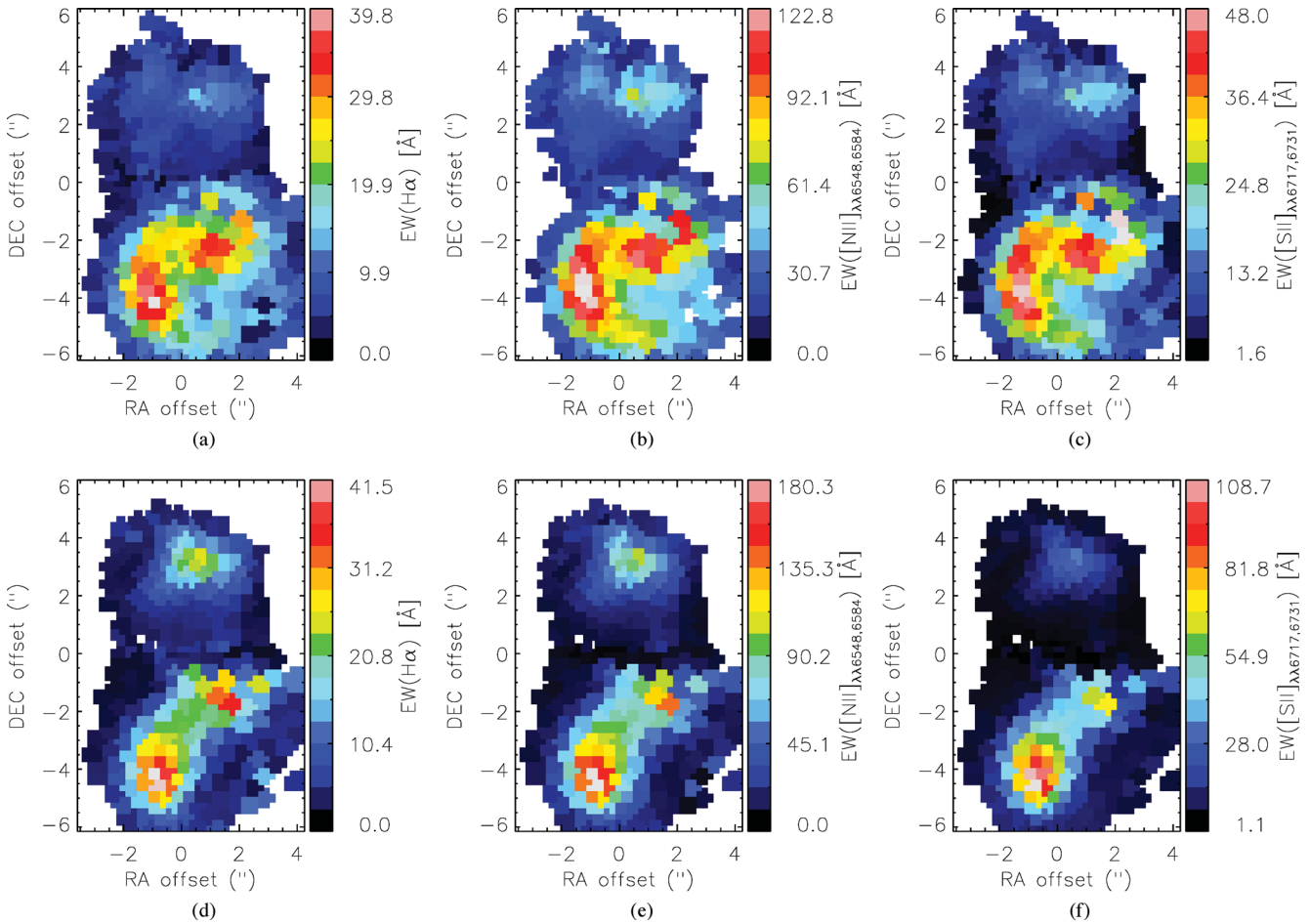

Figure 8. Ionized gas line EWs derived from the GMOS IFU data reduction process discussed in Section 2.2. In the first row we display the EW of component 1 (confined to be closest to the galaxy systemic). Bins where only one ionized gas component is required are also shown in component 1. The EW of the faster outflowing component is shown in the second row. The Hα line EWs are shown in panels a and d, the [N II] line EWs in panels b and e, and the [S II] EWs in panels c and f.

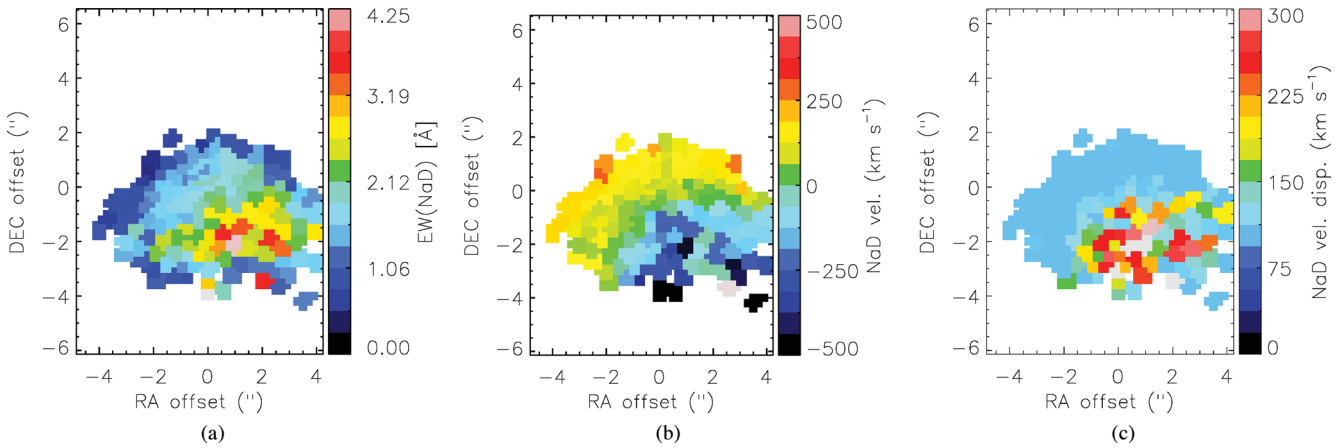

Figure 9. NaD atomic gas kinematics derived from the GMOS IFU data reduction process discussed in Section 2.2.2. In panel a we display the EW of the absorption line. Panel b shows the derived gas kinematics and panel c the derived velocity dispersion.

momentum. The dynamical mass ($M_{1/2}$) of NGC 1266 within a sphere of radius $r_{1/2}$ (containing half of the galaxy light) is 1×10^{10} M$_\odot$ (Cappellari et al., in preparation). A minor merger with a smaller galaxy could provide the gas we see, and with a stellar mass ratio of ≈5:1 (assuming that the smaller galaxy was gas rich, with a gas fraction of 1) it might not leave visible traces in the luminosity-weighted galaxy kinematics.

In Davis et al. (2011) we analysed the kinematic misalignment of the ionized gas in ATLAS^{3D} galaxies (extending the work of Sarzi et al. 2006) in order to gain clues about the origin of the

Downloaded from http://mnras.oxfordjournals.org/ at European Southern Observatory on March 8, 2013

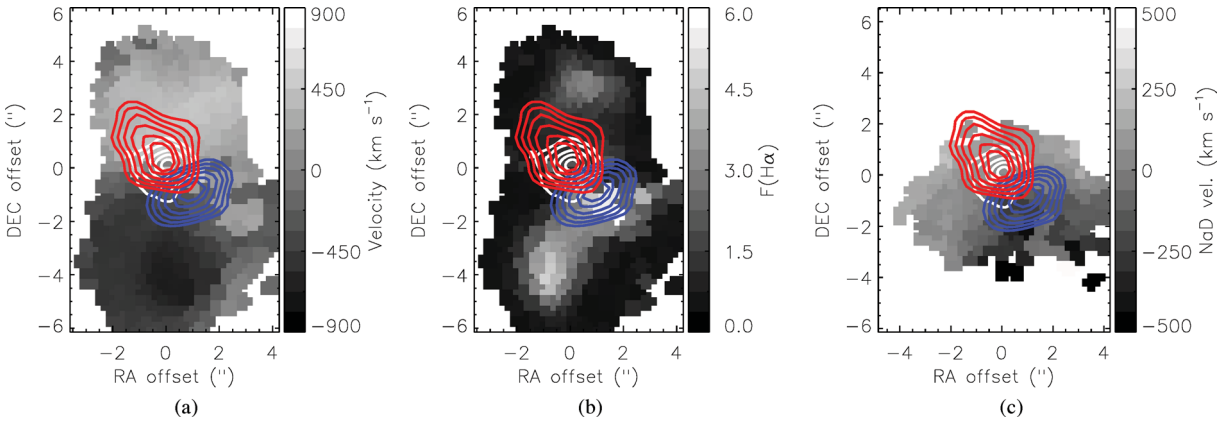

Figure 10. GMOS ionized gas outflow kinematics (panel a), Hα outflow EW (panel b) and NaD kinematics (panel c), as in Figs 7–9 but plotted in grey-scale. These are overplotted with the CO observations of A2011. The white contours show the molecular core, and the blue and red contours the red-shifted and blue-shifted gas, respectively.

gas. In that work we suggested that kinematically misaligned gas almost certainly has an external origin. If the systemic component is rotating (and its misalignment from the stellar rotation axis is not caused by orbit branching or a similar process; Contopoulos & Magnenat 1985; Pfenniger 1985), then this would once again argue for a recent minor merger/accretion.

3.2 NaD absorption

The sodium absorption doublet at 5890 and 5896 Å provides a good probe of the cold ISM in the outflow. The ionization potential of Na I is lower than that of hydrogen, at only 5.1 eV. The photons that ionize Na I are thus in the near-ultraviolet (UV) ($\lambda \approx 2420$ Å). These lines primarily probe the ISM in the warm atomic and cold molecular phases, where there is sufficient dust extinction to allow neutral sodium to survive (Spitzer 1978). For NaD lines to be observed, only relatively modest optical depths and H I column densities are required, which make these lines a sensitive probe of the outflowing (or inflowing) neutral ISM.

As shown in Fig. 9, we detect NaD only in the central regions and the southern part of the galaxy. As absorption lines are viewed against the stellar continuum, if blue-shifted velocities are observed it is clear that the gas is outflowing rather than inflowing. The gas kinematics show that it is likely caught in the outflow, with typical blue-shifted velocities of ≈ -250 km s^{-1} and extreme velocities detected out to -500 km s^{-1} (which are well beyond the escape velocity). The position angle of the outflow traced in NaD (and molecular gas; see Fig. 10) is slightly different than that traced by the ionized gas by $\approx 35^\circ \pm 5^\circ$. It is unclear if the difference between the two gas phases is significant. We further discuss this in Section 3.5.

The presence of NaD in the outflow provides further evidence that NGC 1266 hosts a multiphase outflow and that cold gas is being removed from the galaxy. As discussed above, the outflow extends to higher velocities when traced by ionized gas than when using a dense gas tracer. Either the gas is dissociated further out in the outflow or we no longer have the sensitivity to detect it.

To observe the NaD lines, the extinction must be sufficient for the optical depth (τ) to be $\gtrsim 1$ at 2420 Å which corresponds to an $A_V \gtrsim 0.43$ mag in the V band (for a Cardelli, Clayton & Mathis 1989 extinction law) and to an H I column density of $\gtrsim 8 \times 10^{20}$ cm^{-2}. The NaD lines we observe are likely to be associated with the H I in this source, which is detected in absorption by A2011. They find a total H I column density of $N_{\rm H\,I} = 2.1 \times 10^{21}$ cm^{-2} in front of the continuum source in NGC 1266 and estimate that the H I column depth in the outflow is $\approx 8.9 \times 10^{20}$ cm^{-2}, consistent with our detection of NaD.

Our observations provide an alternative way to estimate the reddening and thus the atomic gas column density in each spaxel. The EW of the NaD absorption lines has been shown to correlate with reddening. Here we use the relation of Turatto, Benetti & Cappellaro (2003), derived from low-resolution spectroscopic observations of supernovae:

$$\frac{E(B-V)}{\rm mag} = -0.01 + 0.16 \times {\rm EW(NaD)}, \quad (1)$$

where $E(B-V)$ is the standard colour excess. This can be combined with the relation between $E(B-V)$ and H I column density, such as that derived by Bohlin, Savage & Drake (1978):

$$\frac{N({\rm H\,I})}{\rm cm^{-2}} = \frac{E(B-V)}{0.2 \times 10^{-21}}. \quad (2)$$

Using these relations we find that the average H I column density in the outflow of NGC 1266, as derived from the NaD EW (displayed in Fig. 9), is $(1.2 \pm 0.6) \times 10^{21}$ cm^{-2}, consistent with the H I absorption spectrum presented in A2011.

The above estimate of N(H I) is very simplistic and assumes that the NaD absorption comes from a 'screen' in front of the galaxy. In fact, due to the small spatial scales we are probing here, some of the stellar continuum detected by GMOS will come from stars in front of the outflow gas, decreasing the measured EW. The amount of contamination will change with radius. Just to the north of the galaxy nucleus, the gas velocity is red-shifted with respect to the galaxy systemic velocity. We are thus likely to see through to the receding part of the outflow. If we assume that the outflow is symmetric, then as we only detect red-shifted material at the very centre, it is implied that the outflow is not in the plane of the galaxy (as otherwise the outflow on the northern side of the galaxy would be silhouetted by the same amount of stellar continuum).

It is possible to use the above facts to introduce a new simple model which can help constrain the geometry of outflows. In this model we treat the inner regions of NGC 1266 as a planar disc, with a vertical scale height of 700 pc. The exact value we choose for the scale height does not critically change our results, so here we adopt a value at the high end of those found for the Milky Way by Chen et al. (2001). As the inner surface brightness profile of NGC 1266 (within ≈ 5 arcsec) is reasonably flat (Krajnovic et al. 2012) in this

Downloaded from http://mnras.oxfordjournals.org/ at European Southern Observatory on March 8, 2013

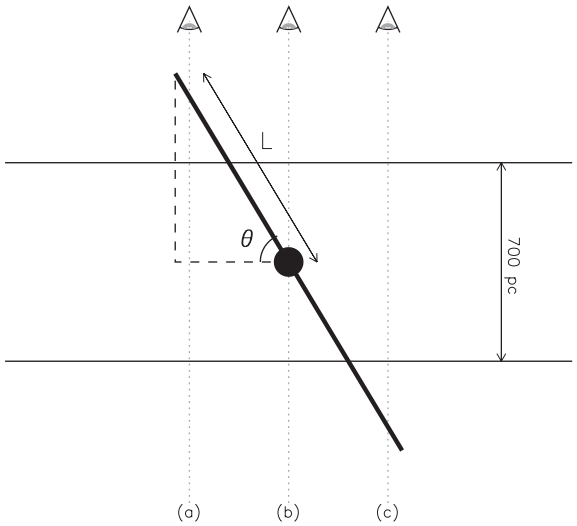

Figure 11. Simple geometry assumed for the NaD absorption model described in Section 3.2. The galaxy is represented as a flat slab with exponentially declining surface density of scale height 700 pc. The outflow has a constant surface density, a variable length (L) and an inclination from the galaxy plane of angle θ. Three sightlines (referred to in the text) are labelled a, b and c.

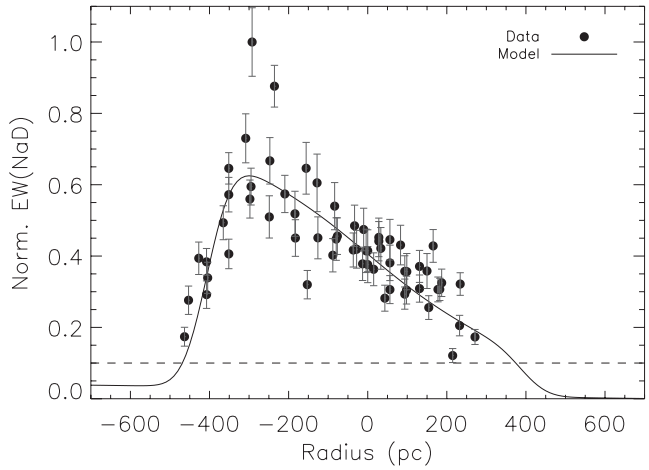

Figure 12. The observed NaD EW distribution (black points) extracted from our GMOS observations in a pseudo-slit of 1 arcsec wide, aligned in the north–south direction over the centre of the galaxy. The solid black line is the best-fitting model for the outflow EW produced in the way described in Section 3.2, convolved with a Gaussian to match the average seeing of our observations. The best model displayed here has an outflow inclination (with respect to the galaxy disc) of 53° and a linear outflow size of 400 pc. The dashed line shows the detection limit of our observations.

simple model, we neglect the change in surface brightness with the radius of the system. We input an outflow with a constant surface density and a variable length (L), which is inclined from the galaxy plane by an angle θ. From equations (1) and (2) we calculate the expected EW(NaD) produced by such an outflow. The measured EW will however be contaminated by the luminosity of the stars between the observer and the absorbing material. At each radius, we calculate the amount of stellar luminosity above and below the position of the outflow and produce a model for the observed EW(NaD) profile.

Fig. 11 demonstrates the model geometry and includes three sightlines as examples of this procedure. In sightline (a) the outflowing material is in front of the majority of the stars in the galaxy, and thus the expected NaD EW will be relatively uncontaminated. Sightline (b) passes through the galaxy centre, and 50 per cent of the stars in the galaxy are in front of the absorbing material; thus, our measured EW will be 50 per cent smaller. Sightline (c) has almost all of the stars in the galaxy in front of the absorber, so the absorption on this sightline is likely undetectable. The exact viewing angle between the galaxy plane and the line of sight introduces a constant geometric factor, which can be neglected when one normalizes the EW profile. The profile shape does not depend on the exact column density assumed for the outflow, and hence this factor is also removed when one normalizes the EW profile.

Models of the above sort can be fitted to the observed NaD EW distribution. Fig. 12 shows the observed NaD EW distribution (black points) extracted from our GMOS observations in a pseudo-slit 1 arcsec wide aligned in the north–south direction over the centre of the galaxy (along what seems to be the major axis of the outflow). Overplotted on the observed data is the best-fitting model for the outflow produced in the way described above (where additionally the model has been convolved with a Gaussian to match the average seeing of our observations). Models with inclinations between 0° and 90°, and with sizes between 1 and 500 pc were created and compared to the data by calculating the reduced chi-squared. The statistical error is calculated by finding the area of parameter space around the best fit where the reduced chi-squared changes by 1. The best-fitting model has an inclination (between the galaxy plane and the outflow) of 53° ± 8° and a size of 400 ± 50 pc. A line corresponding to such a model is shown in Fig. 12.

A2011 estimate the outflow to have a total extent of 465 pc and an inclination with respect to the plane of the sky of roughly 20° (using the average offset between the centroids of the outflow with respect to the nucleus divided by the average extent of the lobes). Using the inclination of 34° ± 5° for the galaxy, as in A2011, combined with our estimate of the outflow inclination (with respect to the galaxy), leads to an estimate of the outflow inclination with respect to the plane of the sky of 18°.5 ± 10°. Both the inclination of the outflow and its size derived from our simple model are thus consistent with the estimates presented in A2011. If we alternatively use the inclination of 26° ± 5° estimated in Davis et al. (2011), within our error bars we still get a result consistent with the estimate of the outflow inclination in A2011.

The conclusion that the outflow in NGC 1266 is orientated out of the plane of the galaxy is supported by the observed kinematic misalignment between the galaxy stellar kinematics, the ionized gas kinematics and the outflow. A2011 also argue that the outflow in NGC 1266 is orientated out of the plane of the galaxy, based on the differential reddening between the northern and southern lobes of ionized gas emission. In Seyfert galaxies, no correlation between the direction of AGN jets and the galactic plane exists (e.g. Ulvestad & Wilson 1984); hence, the misalignment of the outflow in this galaxy is perhaps not unexpected.

Two-parameter models of this type employed here are highly simplistic and ignore a large amount of relevant physics. Despite these reservations, a good fit to observational data can be obtained (as shown in Fig. 12), and the estimated parameters seem reasonable. This highlights the power of NaD observations to constrain the geometry of outflows.

3.3 Gas excitation

Figs 4 and 8 show the distribution of ionized gas in NGC 1266. Ionized gas is detected everywhere in the inner ≈10 arcsec

Downloaded from http://mnras.oxfordjournals.org/ at European Southern Observatory on March 8, 2013

(a projected distance of 1440 pc) of the galaxy; however, the brightness distribution is not smooth. As seen in narrow-band images (and previously discussed in A2011), the ionized gas emission is brighter to the south of the nucleus and has a distinctive 'kidney bowl' shape (best seen in Fig. 8). This structure correlates with the position of the outflow (and with the radio jet; Section 3.5). The asymmetric brightening of the lines is present in both the systemic and outflow components, suggesting that these components are linked in some way. In the rest of this section we use ratios of the line fluxes to understand the ionization mechanism powering this emission.

Using the combination of the SAURON and GMOS IFU data it is possible to construct BPT diagrams (Baldwin et al. 1981) for the inner parts of NGC 1266. In order to use ratios from both data sets, we interpolate the SAURON IFU map on to the GMOS bins. As the SAURON bins are in general larger, some GMOS bins will have identical values of the SAURON line ratios. Fig. 13 shows the [O III]/Hβ ratio derived from our SAURON data, plotted versus the [N II]/Hα (top panel), [S II]/Hα (middle panel) and [O I]/Hα (bottom panel) line ratios from our GMOS observations. In the bottom-right of each plot is the typical error bar associated with each point, derived from the formal fitting errors and a Monte Carlo error analysis of the different fluxes returned by our fitting routines.

On to these diagrams we overplot the diagnostic lines of Kewley et al. (2001, 2006), which indicate the dominant line excitation mechanism. In all of the panels, it is clear that star formation cannot excite the lines we see in NGC 1266. The top diagram shows that the gas is ionized either by an AGN or by shock processes. The middle and bottom panels show that the majority of the spaxels have line ratios which are consistent with low-ionization nuclear emission region (LINER; Heckman 1980) like activity. LINERs are a controversial classification (see Ho 2008 for a review), with some authors claiming that the ionization comes from an AGN (e.g. Ferland & Netzer 1983; Ho, Filippenko & Sargent 1993), fast shocks (Burbidge, Gould & Pottasch 1963; Dopita & Sutherland 1995) or photoionization by UV bright stellar sources (di Serego Alighieri, Trinchieri & Brocato 1990; Binette et al. 1994; O'Dea et al. 2010; Sarzi et al. 2010).

In addition to the BPT diagrams, it is also possible to plot the observed line ratios over grids that predict the line ratios of ionized gas lines in given scenarios. Both obscured and unobscured AGN models from Groves, Dopita & Sutherland (2004) fail to fully reproduce the observed line ratios. The closest AGN model requires a metallicity of $4\,Z_{\odot}$, an electron density of $1000\,\mathrm{cm}^3$ and a relatively constant radiation field. Even then this model cannot fully reproduce the observed line ratio distribution. We find that the only model that can reproduce the emission line ratios we observe is a shock model from Allen et al. (2008), again with a super-solar metallicity ($\approx 2\,Z_{\odot}$). The stars in NGC 1266 have a sub-solar metallicity (McDermid et al., in preparation), and thus if the gas really is of super-solar metallicity, then it must have been significantly enriched.

Fig. 14 shows our best-fitting shock models from the SAURON-specific line ratio diagram [O III]/Hβ versus [N I]/Hα and the SAURON/GMOS combined [O III]/Hβ versus [S II]/Hα and [O I]/Hα diagrams. The emission observed requires shock velocities of up to $\approx$800 km s^{-1} and an average magnetic field of $\approx$3 μG cm$^{3/2}$. The shock velocities are similar to the outflow velocities, suggesting that the shocked emission is powered by the outflow.

The shock velocities derived from these grids are highest at the centre and towards the northern (red-shifted) side of the outflow (see panel a of Fig. 15). This is true in all the data sets, even though the line ratio that drives the shock determination is different.

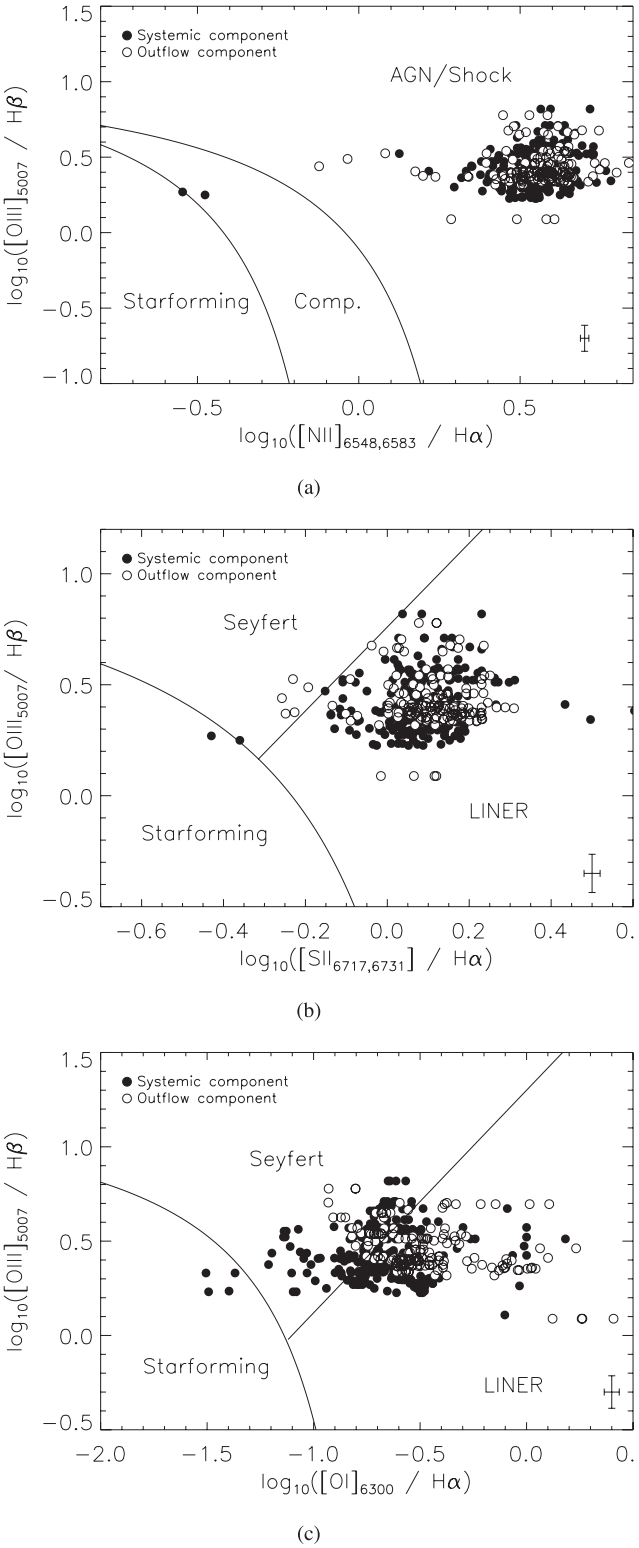

Figure 13. BPT (Baldwin, Phillips & Terlevich 1981) type diagrams for the inner parts of NGC 1266. The *y*-axis of each plot shows the [O III]/Hβ ratio derived from our SAURON data, and it is plotted versus the [N II]/Hα (panel a; top), [S II]/Hα (panel b; middle) and [O I]/Hα (panel c; bottom) line ratios from our GMOS observations. In the bottom-right of each plot is the typical error bar associated with each point, derived from the formal fitting errors and a Monte Carlo error analysis of the fluxes returned by our fitting routines. We overplot the diagnostic lines of Kewley et al. (2001, 2006), which indicate the dominant line excitation mechanism.

Downloaded from http://mnras.oxfordjournals.org/ at European Southern Observatory on March 8, 2013

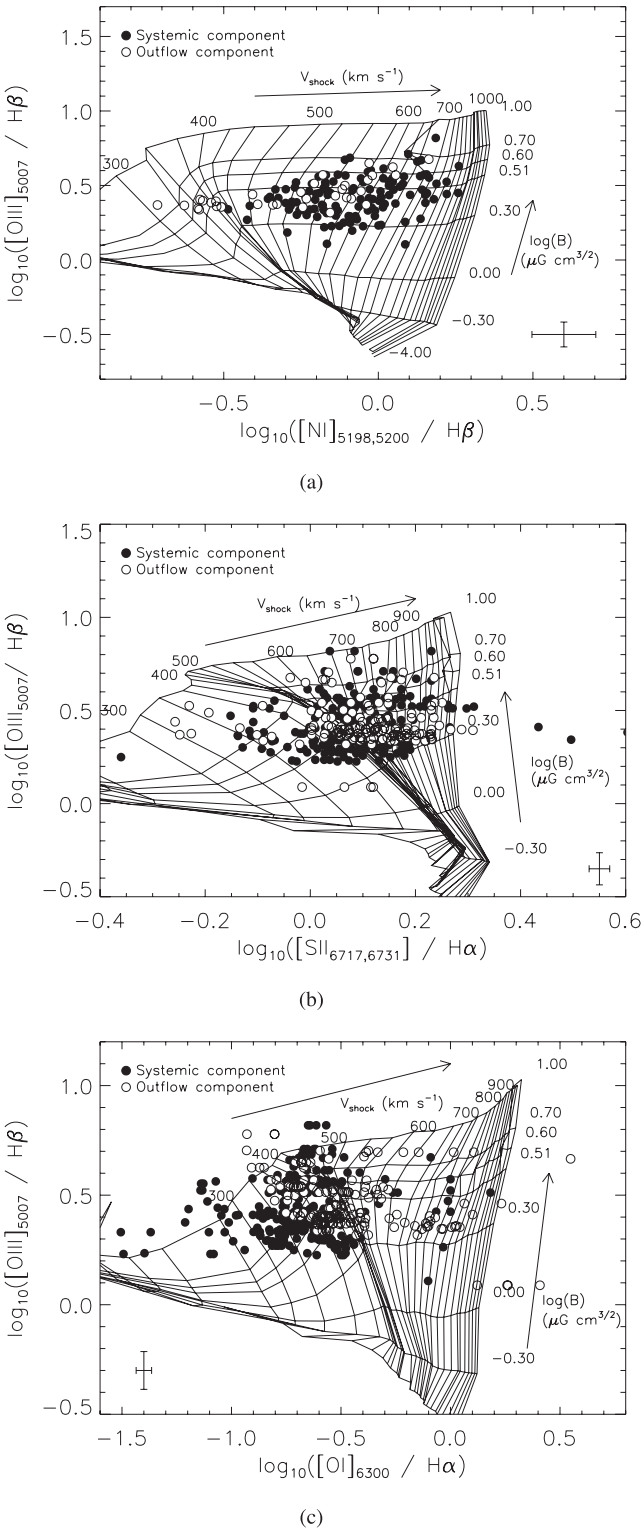

Figure 14. Observed line ratios for spaxels in the inner parts of NGC 1266, plotted over a shock model with a super-solar metallicity ($\approx 2\,Z_{\odot}$), taken from Allen et al. (2008). The *y*-axis of each plot shows the [O III]/Hβ ratio derived from our SAURON data, and it is plotted versus the [N II]/Hα (panel a; top), [S II]/Hα (panel b; middle) and [O I]/Hα (panel c; bottom) line ratios from our GMOS observations. In the bottom of each plot is the typical error bar associated with each point, derived from the formal fitting errors and a Monte Carlo error analysis of the fluxes returned by our fitting routines.

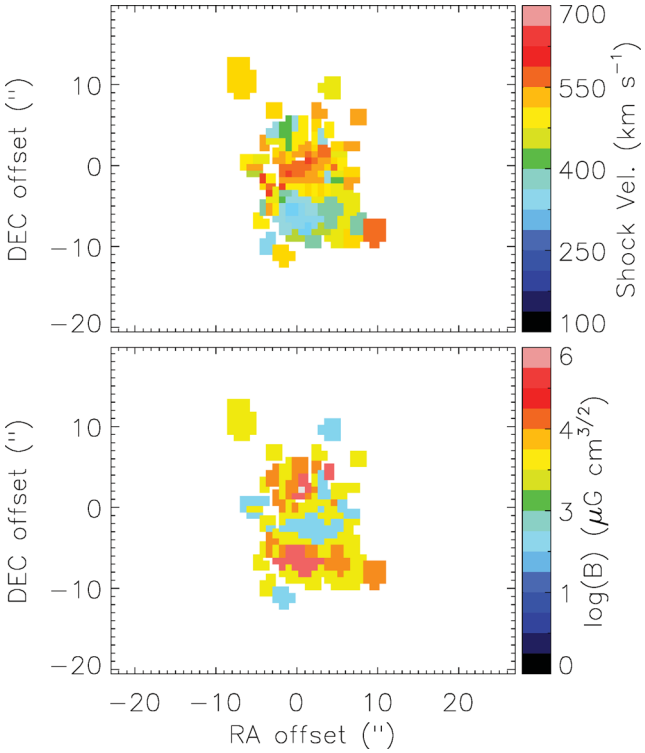

Figure 15. Shock velocities (top panel) and magnetic field strengths (bottom panel) for the systemic component derived from the SAURON-only [O III]/Hβ versus [N I]/Hα diagram by interpolating the shock grid presented in Fig. 14. The same trends are observed in the mixed GMOS/SAURON diagrams.

The [S II]/Hα grid predicts higher shock velocities than the [N I]/Hα grid, but the average shock velocity is consistent. The [O I]/Hα grid predicts lower shock velocities on average, but this is driven by the bins that fall within the Seyfert region of the associated BPT diagram (Fig. 13). These spaxels are mostly located in the centre of the galaxy, where the AGN contribution to the ionization is likely to be the strongest. It is not surprising that suggestions of the embedded AGN are most clearly seen in the [O I]/Hα diagram, as the presence of strong [O I]λ6300 is usually indicative of a power-law ionizing spectrum. The [O I] line, which is collisionally excited, will only occur in a zone which has a sufficiently high electron density and temperature to excite the upper level. With a stellar input spectrum, these conditions only occur within the H^+ Strömgren sphere, where the O^0 abundance is negligible. However, a gas ionized by a relatively flat power-law spectrum has an extended partially ionized zone where the [O I] emission arises (Peterson 1997).

The magnetic field appears to increase with increasing distance from the centre of the galaxy, perhaps due to compression of magnetic field lines as they enter the shocked gas (panel b; Fig. 15). Shock velocities are similar in both the systemic and outflow components, again arguing that these components are linked, but the magnetic field may be higher, on average in the outflowing component.

A2011 have shown that NGC 1266 has a deeply embedded AGN, but as we show here, the ionized gas emission in this LINER galaxy is dominated by shocks, likely caused by the outflow. A similar shocked, high-metallicity wind has been postulated to explain the LINER-like emission from starburst superwinds (e.g. Rich et al. 2010). The shocks in NGC 1266 exist at high velocities, similar

Downloaded from http://mnras.oxfordjournals.org/ at European Southern Observatory on March 8, 2013

to those found in the outflow, once again demonstrating the link between the ionized gas and the material in the outflow.

3.4 Physical conditions

Using the ionized gas lines we detect, it is possible to estimate the physical conditions within the ionized gas in each spaxel. From the ratio of the 6731 and 6717 Å lines in the [S II] doublet, it is possible to estimate the luminosity-weighted electron density along each line of sight. The ratio of the [N II] doublet at λλ6548, 6584 Å and the [N II] line at λ5755 Å also provides a sensitive temperature tracer that depends very little upon the density of the gas. We calculated these line ratios for each spaxel where it is constrained by our GMOS data and used the NEBULAR package in IRAF to estimate the electron density and temperature, based on the five-level atom program developed by De Robertis et al. (1987).

Fig. 16 shows maps of the derived electron density for the systemic and outflow components, and a histogram of the bin values in both components. In significant areas of the outflow component, the [S II] ratio is saturated at the low-density limit. As shown in panel b of Fig. 16, however, in the highest velocity regions of the outflow where the line ratio is not saturated, the average density is higher than that in the systemic component. The required lines to calculate the electron temperature were detected in fewer spaxels, and so we do not reproduce these plots here. However, a reasonably consistent picture emerges, with the higher density outflow having lower average temperature and vice versa for the lower density systemic component. We hypothesize that the outflow may be of higher average density due to a pile-up of material in-front of the ionized gas shock, and/or an increase in the number of free electrons due to ionization from the shock. The disturbed structure in the systemic component appears to have a lower electron density than the rest of the gas, on average, supporting the hypothesis that this could be a different gas component.

The northern half of the ionized gas systemic component has a lower electron density, on average, than the southern half. Some of the ionized gas densities in the northern regions are even at the low-density limit. This could potentially offer an explanation for some of the puzzling features of the outflow. If the ISM is unevenly distributed on each side of the nucleus, then the same input energy from the central engine would dissipate faster in the denser material, producing stronger line emission in the denser southern regions, as observed. The lower density in the northern region would allow the same energy input to produce a faster shock, as observed. The magnetic field in the northern region may also be lower, and this would decrease the expected synchrotron flux from a jet, as observed in Section 3.5. One might however expect that the outflow would thus be faster on the northern side of the nucleus, as the outflowing material would encounter less resistance. This is not observed in the velocity fields presented in this paper.

The observable tracers of the outflow that we currently possess (ionized and atomic gas in this paper, molecular gas in A2011) however have to be present at sufficient densities to be detectable, and more sensitive observations may be required to detect the highest velocity parts of the red-shifted outflow. Both evidence from A2011 and that from the NaD absorption presented in this paper suggest that the red-shifted northern part of the outflow is seen through the galaxy, and dust obscuration could potentially prevent us from detecting low-level ionized gas emission.

3.5 Driving mechanisms

The physical mechanism by which an AGN removes gas from a galaxy is still widely debated. As discussed above, radiation pressure, broad-line winds, cosmic ray heating and radio jets have all been mooted as potential methods for driving gas out of galaxies. In NGC 1266, the gas is clearly being accelerated and removed from the galaxy, and the cold gas phase survives reasonably far out into the outflow. A2011 argue that radiation-driven winds are unable to provide enough mechanical energy to drive the outflow, and thus an AGN jet is a more likely driving mechanism. 1.4 and 5 GHz radio continuum maps are available for NGC 1266 (Baan & Klöckner 2006) and are shown in Fig. 17. The 1.4 GHz image shows a central bright point source and a jet-like extension to the south and north.

A similar jet-like structure is visible in the 5 GHz image, but in this higher resolution image the emission to the south and north of the nucleus is not connected to the point source. This lack of connection could be real, or because the Very Large Array observations used here have resolved out the connecting structure. We could be

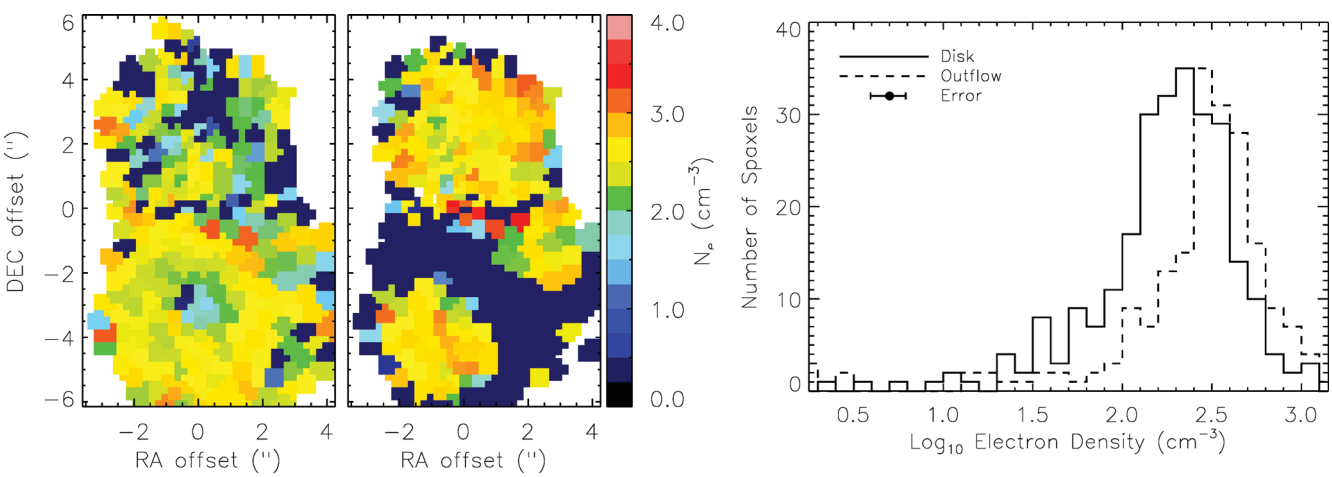

(a) (b)

Figure 16. Panel a shows maps of the electron density (in log units), derived from the [S II] doublet, within the systemic component (left) and outflow (right-hand panel) of NGC 1266. Panel b shows a histogram of the electron density from the non-saturated bins, for the systemic component (solid line) and the outflow (dashed line). The median error in the electron density is shown in the legend.

Downloaded from http://mnras.oxfordjournals.org/ at European Southern Observatory on March 8, 2013

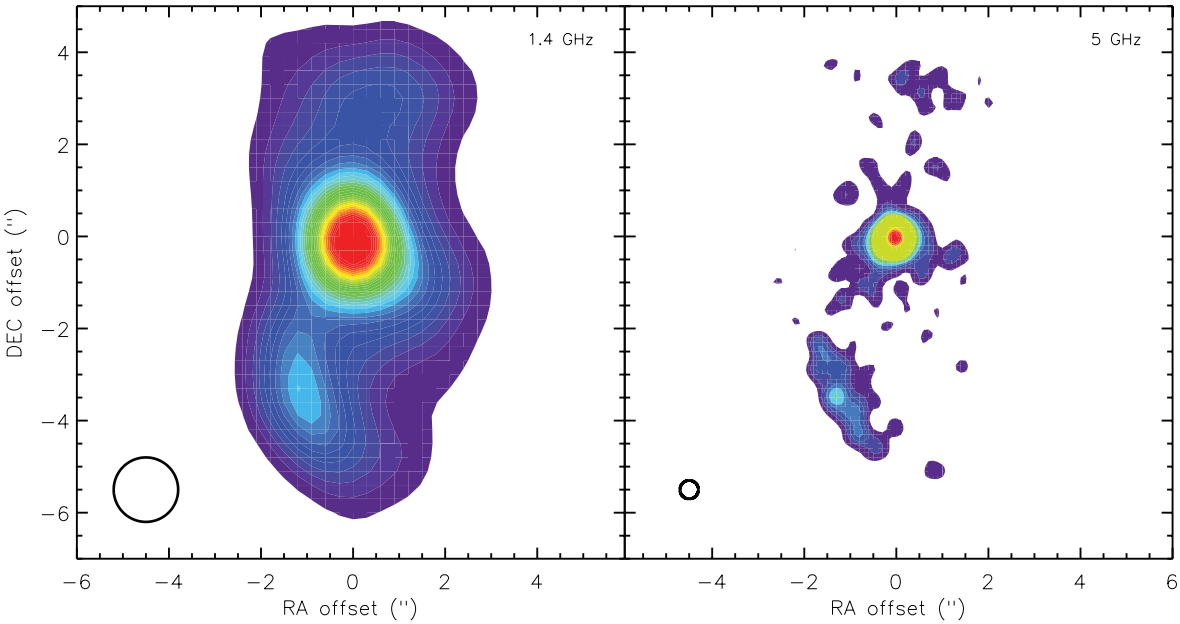

Figure 17. 1.4 and 5 GHz radio continuum maps of the centre of NGC 1266 from Baan & Klöckner (2006). The maps are shown for all emission above 5σ (1.4 GHz) and 3σ (5 GHz) with contours spaced by 1σ. The beam sizes of ≈1.5 arcsec and ≈0.4 arcsec, respectively, are indicated in the figures in the bottom-left. NGC 1266 has an integrated flux density of 90.34 ± 2.83 mJy at 1.4 GHz (Alatalo et al., in preparation).

seeing emission from where the jet hits the surrounding ISM (cf. hot spots), or the jet itself may contain discrete blobs of synchrotron emitting plasma.

The central source in this object appears to be driving the outflow, despite being a low-luminosity AGN (having a total radio power at 5 GHz of $\lesssim 10^{22}$ W Hz^{-1}; Alatalo et al., in preparation). This highlights that low-luminosity AGN may also be important sources of feedback. The spectral index of the central point source (which is unlikely to be affected by *uv*-coverage issues) has a spectral index typical of an low-luminosity AGN source (α[1.4–5 GHz] ≈ −0.66; Alatalo et al., in preparation). The spectral index when including the outer structures steepens (α[1.4–5 GHz] ≈ −0.79), as is seen in hot spots in local radio galaxies (e.g. Hoekstra, Barthel & Hes 1997), but as some emission could have been resolved out, we cannot be sure if this value is robust.

Fig. 18 shows the 1.4 GHz radio continuum structure overplotted on our GMOS maps of the ionized gas and neutral gas outflows. The observed radio structure correlates well with the features observed in the ionized and atomic gas. The radio morphology is similar to that predicted by models of disrupted Fanaroff–Riley type I objects, as expected given the very dense environment around the jet, where it can be rapidly decelerated and disrupted by gas entrainment (e.g. Laing & Bridle 2002; Laing et al. 2011).

The 'kidney-bowl' shock structure observed in the ionized gas traces well the southern edge of the jet seen in radio continuum, as is observed in many radio galaxies (i.e. the 'alignment effect'; Chambers, Miley & van Breugel 1987; McCarthy et al. 1987). This suggests that the shock suggested by the ionized gas line ratios occurs where the radio plasma impacts with the ionized gas. The blue-shifted feature on the south-eastern side of the systemic component also seems to correlate well with the jet. This feature may well be associated with the jet, arguing that the systemic component may not represent a single structure.

The radio continuum structure hooks around the fastest moving neutral and ionized gas. As discussed above, the position angle of the outflow traced in NaD (and molecular gas; see Fig. 10) is slightly different than that traced by the ionized gas. Projection effects could possibly explain some of the differences between the position angles, but it is unclear if this can completely remove the discrepancy. If this effect is real, then it could potentially arise because interaction with the ISM has deflected the jet, or the jet could be precessing (as observed, e.g., in Cen A; Haynes, Cannon & Ekers 1983). Of course, it is also possible that the jet itself is powering the ionized gas outflow, but another mechanism (e.g. winds or radiation pressure) could be driving the atomic and molecular outflows, naturally leading to different position angles (see, e.g., Rupke & Veilleux 2011). From the speed of the outflow and its measured extent, we can estimate the lifetime of the phenomenon. Both the ionized gas (extending to ≈1.5 kpc and travelling at up to 900 km s^{-1}) and the neutral gas (extending to ≈400 pc and travelling at an average of 250 km s^{-1}) give a similar estimate for the lifetime of the outflow (≈1.6 Myr). This would seem to suggest that the outflows in ionized and neutral gas have a common cause. Radiation pressure driving the outflow also seems unlikely on energetics grounds (see A2011). Deep high-resolution observations of the radio continuum structure could help distinguish the cause of this effect.

4 CONCLUSIONS

In this paper we have been able to shed some light on the outflow activity in NGC 1266. This unusual galaxy is relatively nearby, allowing us to investigate the process of AGN feedback in action. Using the SAURON and GMOS IFUs we detected strong ionized gas emission lines (Hα, Hβ, [O III], [O I], [N II], [S II] and He I), as well as NaD absorption. We use these tracers to explore the structure of the source, derive the ionized and atomic gas kinematics and investigate the gas excitation and physical conditions.

NGC 1266 contains two ionized gas components along each line of sight, tracing the ongoing outflow and a component closer to the galaxy systemic, the origin of which is unclear. The gas appears to be disturbed by a nascent AGN jet.

Downloaded from http://mnras.oxfordjournals.org/ at European Southern Observatory on March 8, 2013

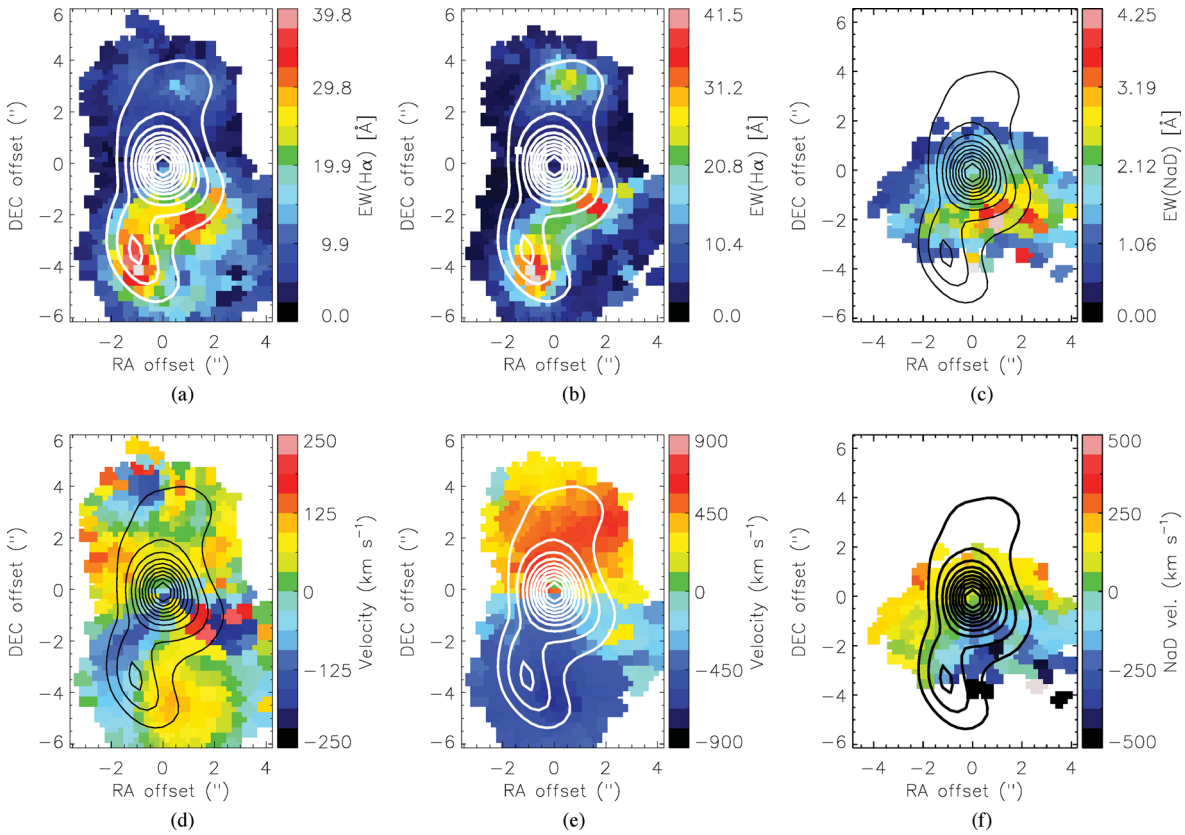

Figure 18. 1.4 GHz radio emission contours (spaced every 8 per cent from 90 to 8 per cent of the peak flux) overplotted on Hα flux maps for the systemic and the outflow components (panels a and b), velocity fields for the systemic and the outflow components (panels d and e) and NaD neutral gas EW and kinematics (panels c and f).

We have presented further evidence that the outflow in this object is truly multiphase, containing radio emitting plasma, ionized and atomic gas, as well as the molecular gas and X-ray emitting plasma (as detected in A2011). With outflow velocities of up to 900 km s^{-1}, the outflow is very likely to remove significant amount of cold gas from the galaxy. The ionized gas morphology correlates well with the radio jets observed in 1.4 and 5 GHz continuum emission, supporting the suggestion of A2011 that an AGN jet is the most likely driving mechanism for the ionized gas outflow.

The line emission in NGC 1266 makes it to be classified as a LINER in optical diagrams. We show here that although NGC 1266 undoubtedly hosts an AGN (see A2011), the line emission in this object is extended and is most consistent with excitation from fast shocks caused by the interaction of the radio jet with the ISM. These shocks have velocities of up to 800 km s^{-1}, which match well with the observed velocity of the outflow.

Using the observed NaD absorption we are able to set further constraints on the size and orientation of the outflow. We show that we are able to detect atomic gas entrained in the outflow out to a (deprojected) distance of $\approx$400 $\pm$ 50 pc and that the outflow has an inclination (between the galaxy plane and the outflow) of 53° $\pm$ 8°. This suggests that the outflow is misaligned from the stellar body. Furthermore, we are able to provide an independent estimate of the column density of neutral material in the outflow $N_{\rm H\,I} = (1.2 \pm 0.6) \times 10^{21}$ cm^{-2}. This estimate is consistent with that derived from H I absorption in A2011. The neutral and molecular outflows are well correlated, but appear to be outflowing along a slightly different axis to the ionized gas. The cause of this effect is unclear.

NGC 1266 is a highly complex object, and it is clear that further observations will be required to fully understand it. Observations of single emission lines (either with an IFU or with a Fabry–Pérot instrument) will be important to overcome problems with line blending inherent in this high velocity dispersion source. Higher spatial resolution would also be advantageous to obtain clear diagnostics of AGN activity and to better understand the shock structure. Sensitive interferometric radio observations at high angular resolution would also enable us to understand the morphology and orientation of the nascent radio jet. The Atacama Large Millimeter/sub-millimeter Array (ALMA) will allow us to study the molecular component of the outflow in greater detail and to further determine the driving mechanism. For instance, if molecular shock tracers are found predominantly in the outflow, then a kinetic driving mechanism would be favoured, while if photon-dominated region tracing species were detected, this would argue for a radiation-driven component to the outflow.

This galaxy is one of the few currently known in which we can witness ongoing active feedback, where a central AGN is disrupting its star-forming reservoir. It is clear that understanding the processes removing the ISM will have widespread applications to both theoretical and observational attempts to understand AGN feedback, its effect on the ISM and its role in building up the red sequence.

ACKNOWLEDGMENTS

The authors thank the referee, Katherine Inskip, for comments which improved the paper. TAD thanks Millie Maier, Niranjan Thatte, Mark Westmoquette and Grant Tremblay for useful

Downloaded from http://mnras.oxfordjournals.org/ at European Southern Observatory on March 8, 2013

discussions. The research leading to these results has received funding from the European Community's Seventh Framework Programme (/FP7/2007-2013/) under grant agreement no 229517.

The SAURON observations were obtained at the WHT, operated by the Isaac Newton Group in the Spanish Observatorio del Roque de los Muchachos on La Palma, Canary Islands. This work is also based on observations obtained at the Gemini Observatory, which is operated by the Association of Universities for Research in Astronomy, Inc., under a cooperative agreement with the NSF on behalf of the Gemini partnership: the National Science Foundation (United States), the Science and Technology Facilities Council (United Kingdom), the National Research Council (Canada), CONICYT (Chile), the Australian Research Council (Australia), Ministrio da Cincia, Tecnologia e Inovao (Brazil) and Ministerio de Ciencia, Tecnologa e Innovacin Productiva (Argentina). RMcD is also supported by the Gemini Observatory.

This work was supported by the rolling grants 'Astrophysics at Oxford' PP/E001114/1 and ST/H002456/1 and visitors grants PPA/V/S/2002/00553, PP/E001564/1 and ST/H504862/1 from the UK Research Councils. RLD acknowledges travel and computer grants from Christ Church, Oxford and support from the Royal Society in the form of a Wolfson Merit Award 502011.K502/jd. RLD also acknowledges the support of the ESO Visitor Programme which funded a three-month stay in 2010.

MC acknowledges support from a Royal Society University Research Fellowship. SK acknowledges support from the Royal Society Joint Projects Grant JP0869822. TN and MB acknowledge support from the DFG Cluster of Excellence 'Origin and Structure of the Universe'. MS acknowledges support from an STFC Advanced Fellowship ST/F009186/1. PS is an NWO/Veni fellow. MB has received, during this research, funding from the European Research Council under the Advanced Grant Program Num 267399-Momentum. The authors acknowledge financial support from ESO.

REFERENCES

Acker A., Köppen J., Samland M., Stenholm B., 1989, Messenger, 58, 44
Alatalo K. et al., 2011, ApJ, 735, 88 (A2011)
Allen M. G., Groves B. A., Dopita M. A., Sutherland R. S., Kewley L. J., 2008, ApJS, 178, 20
Allington-Smith J. et al., 2002, PASP, 114, 892
Arav N., Korista K. T., de Kool M., Junkkarinen V. T., Begelman M. C., 1999, ApJ, 516, 27
Baan W. A., Klöckner H.-R., 2006, A&A, 449, 559
Bacon R. et al., 1995, A&AS, 113, 347
Bacon R. et al., 2001, MNRAS, 326, 23
Baldry I. K., Glazebrook K., Brinkmann J., Ivezić Ž., Lupton R. H., Nichol R. C., Szalay A. S., 2004, ApJ, 600, 681
Baldwin J. A., Phillips M. M., Terlevich R., 1981, Astron. Soc. Pac., 93, 5
Begelman M., de Kool M., Sikora M., 1991, ApJ, 382, 416
Binette L., Magris C. G., Stasińska G., Bruzual A. G., 1994, A&A, 292, 13
Bohlin R. C., Savage B. D., Drake J. F., 1978, ApJ, 224, 132
Burbidge G. R., Gould R. J., Pottasch S. R., 1963, ApJ, 138, 945
Cappellari M., Copin Y., 2003, MNRAS, 342, 345
Cappellari M., Emsellem E., 2004, PASP, 116, 138
Cappellari M. et al., 2011, MNRAS, 413, 813 (ATLAS^{3D} Paper I)
Cardelli J. A., Clayton G. C., Mathis J. S., 1989, ApJ, 345, 245
Chambers K. C., Miley G. K., van Breugel W., 1987, Nat, 329, 604
Chen B. et al., 2001, ApJ, 553, 184
Contopoulos G., Magnenat P., 1985, Celest. Mech., 37, 387
Croton D. J. et al., 2006, MNRAS, 365, 11
Davis T. A. et al., 2011, MNRAS, 414, 968
Davis T. A. et al., 2011, MNRAS, 417, 882
De Robertis M. M., Dufour R. J., Hunt R. W., 1987, J. R. Astron. Soc. Can., 81, 195
di Serego Alighieri S., Trinchieri G., Brocato E., 1990, in Fabbiano G., Gallagher J. S., Renzini A., eds, Astrophys. Space Sci. Lib., Vol. 160, Windows on Galaxies. Kluwer, Dordrecht, p. 301
Dimitrijević M. S., Popović L. Č., Kovačević J., Dačić M., Ilić D., 2007, MNRAS, 374, 1181
Dopita M. A., Sutherland R. S., 1995, ApJ, 455, 468
Emsellem E. et al., 2004, MNRAS, 352, 721
Ferland G. J., Netzer H., 1983, ApJ, 264, 105
Ferland G. J., Fabian A. C., Hatch N. A., Johnstone R. M., Porter R. L., van Hoof P. A. M., Williams R. J. R., 2009, MNRAS, 392, 1475
Groves B. A., Dopita M. A., Sutherland R. S., 2004, ApJS, 153, 75
Haynes R. F., Cannon R. D., Ekers R. D., 1983, Astron. Soc. Aust., 5, 241
Heckman T. M., 1980, A&A, 87, 152
Ho L. C., 2008, ARA&A, 46, 475
Ho L. C., Filippenko A. V., Sargent W. L. W., 1993, ApJ, 417, 63
Hoekstra H., Barthel P. D., Hes R., 1997, A&A, 319, 757
Hook I. M., Jørgensen I., Allington-Smith J. R., Davies R. L., Metcalfe N., Murowinski R. G., Crampton D., 2004, PASP, 116, 425
Kennicutt R. C., Jr, et al., 2003, PASP, 115, 928
Kewley L. J., Dopita M. A., Sutherland R. S., Heisler C. A., Trevena J., 2001, ApJ, 556, 121
Kewley L. J., Groves B., Kauffmann G., Heckman T., 2006, MNRAS, 372, 961
Krajnović D. et al., 2011, MNRAS, 414, 2923 (ATLAS^{3D} Paper II)
Krajnović D. et al., 2012, MNRAS, submitted
Kurosawa R., Proga D., 2009, MNRAS, 397, 1791
Laing R. A., Bridle A. H., 2002, MNRAS, 336, 1161
Laing R. A., Guidetti D., Bridle A. H., Parma P., Bondi M., 2011, MNRAS, 417, 2789
Markwardt C. B., 2009, in Bohlender D., Dward D., Dowler P., ASP Conf. Ser. Vol. 411, Astronomical Data Analysis Software and Systems XVIII. Astron. Soc. Pac., San Francisco, p. 251
McCarthy P. J., van Breugel W., Spinrad H., Djorgovski S., 1987, ApJ, 321, L29
McNamara B. R., Nulsen P. E. J., 2012, New J. Phys., 14, 055023
Murray N., Quataert E., Thompson T. A., 2005, ApJ, 618, 569
O'Dea K. P. et al., 2010, ApJ, 719, 1619
Ostriker J. P., Choi E., Ciotti L., Novak G. S., Proga D., 2010, ApJ, 722, 642
Peterson B. M., 1997, An Introduction to Active Galactic Nuclei. Cambridge Univ. Press, Cambridge
Pfenniger D., 1985, A&A, 150, 97
Rich J. A., Dopita M. A., Kewley L. J., Rupke D. S. N., 2010, ApJ, 721, 505
Rosario D. J., Shields G. A., Taylor G. B., Salviander S., Smith K. L., 2010, ApJ, 716, 131
Rupke D. S. N., Veilleux S., 2011, ApJ, 729, L27
Sarzi M. et al., 2006, MNRAS, 366, 1151
Sarzi M. et al., 2010, MNRAS, 402, 2187
Schawinski K., Thomas D., Sarzi M., Maraston C., Kaviraj S., Joo S.-J., Yi S. K., Silk J., 2007, MNRAS, 382, 1415
Spitzer L., 1978, Physical Processes in the Interstellar Medium. Wiley Interscience, New York
Springel V., Di Matteo T., Hernquist L., 2005, ApJ, 620, L79
Storey P. J., Zeippen C. J., 2000, MNRAS, 312, 813
Turatto M., Benetti S., Cappellaro E., 2003, in Hillebrandt W., Leibundgut B., eds, Proc. ESO/MPA/MPE Workshop, From Twilight to Highlight: The Physics of Supernovae. Springer-Verlag, Berlin, p. 200
Ulvestad J. S., Wilson A. S., 1984, ApJ, 285, 439
van de Ven G., Falcon-Barroso J., McDermid R. M., Cappellari M., Miller B. W., de Zeeuw P. T., 2010, ApJ, 719, 1481
Young L. M. et al., 2011, MNRAS, 414, 940

This paper has been typeset from a TEX/LATEX file prepared by the author.

Downloaded from http://mnras.oxfordjournals.org/ at European Southern Observatory on March 8, 2013